(2)

RESEARCH INTO MBE FOR USE IN PHOTOVOLTAIC DIODE DETECTORS

O.K. Wu and G.S. Kamath

Hughes Research Laboratories
3011 Malibu Canyon Road
Malibu, California 90265

March 1989

DAAB07-86-C-F019
Final Report
September 16, 1986 through December 31, 1988

U.S. ARMY COMMUNICATIONS-ELECTRONICS COMMAND
NIGHT VISION AND ELECTRO-OPTICS LABORATORY
Ft. Belvoir, VA 22060-5677

REPORT DOCUMENTATION PAGE

Form Approved
OMB No. 0704-0188

1a. REPORT SECURITY CLASSIFICATION: Unclassified	1b. RESTRICTIVE MARKINGS
2a. SECURITY CLASSIFICATION AUTHORITY	3. DISTRIBUTION / AVAILABILITY OF REPORT
2b. DECLASSIFICATION / DOWNGRADING SCHEDULE	
4. PERFORMING ORGANIZATION REPORT NUMBER(S)	5. MONITORING ORGANIZATION REPORT NUMBER(S)
6a. NAME OF PERFORMING ORGANIZATION: Hughes Research Laboratories; 6b. OFFICE SYMBOL (If applicable): HRL	7a. NAME OF MONITORING ORGANIZATION: U.S. Army Communications-Electronics Command Night Vision and Electro-Optical Laboratory
6c. ADDRESS (City, State, and ZIP Code): 3011 Malibu Canyon Road, Malibu, California 90265	7b. ADDRESS (City, State, and ZIP Code): Fort Belvoir, VA 22060-5677
8a. NAME OF FUNDING / SPONSORING ORGANIZATION; 8b. OFFICE SYMBOL (If applicable)	9. PROCUREMENT INSTRUMENT IDENTIFICATION NUMBER: DAAB07-86-C-F019
8c. ADDRESS (City, State, and ZIP Code): Fort Belvoir, VA 22060-5677	10. SOURCE OF FUNDING NUMBERS: PROGRAM ELEMENT NO. / PROJECT NO. / TASK NO. / WORK UNIT ACCESSION NO

11. TITLE (Include Security Classification)

RESEARCH INTO MBE FOR USE IN PHOTOVOLTAIC DIODE DETECTORS (U)

12. PERSONAL AUTHOR(S)
Wu, O.K. and Kamath, G.S.

13a. TYPE OF REPORT	13b. TIME COVERED	14. DATE OF REPORT (Year, Month, Day)	15. PAGE COUNT
Final	FROM 86/9/16 TO 88/12/31	1989 March 3	60

16. SUPPLEMENTARY NOTATION

17. COSATI CODES			18. SUBJECT TERMS (Continue on reverse if necessary and identify by block number)
FIELD	GROUP	SUB-GROUP	MBE HgCdTe layers, chemical doping n-type and p-type, optical and electrical properties, double layer heterojunctions

19. ABSTRACT (Continue on reverse if necessary and identify by block number)

Substantial progress has been made in several critical areas of the program. We have established a strong MBE capability for growing device quality HgCdTe layers required for IR detector fabrication. The MBE system has been systematically modified and state-of-the-art layers of HgCdTe with excellent control in composition and semiconductor properties have been grown. A breakthrough in p-type doping has been achieved, which has led to the controlled growth of extrinsically p-type layers of HgCdTe doped with arsenic in the range of 10^{15} to 10^{18} cm^{-3} that remain p-type even after mercury anneal. Controlled n-type doping of HgCdTe achieved by using indium in the range of 10^{18} to 10^{16} cm^3 with mobilities of $2x10^4$ to $8x10^3$ $cm^2/V \cdot s$. Several double layer heterojunction structures were grown and 8 mil by 9 mil diodes were fabricated and tested.

20. DISTRIBUTION / AVAILABILITY OF ABSTRACT	21. ABSTRACT SECURITY CLASSIFICATION
☐ UNCLASSIFIED/UNLIMITED ☐ SAME AS RPT ☐ DTIC USERS	Unclassified
22a. NAME OF RESPONSIBLE INDIVIDUAL	22b. TELEPHONE (Include Area Code) / 22c. OFFICE SYMBOL

TABLE OF CONTENTS

LIST OF ILLUSTRATIONS

LIST OF ILLUSTRATIONS (Continued)

LIST OF TABLES

SECTION 1

INTRODUCTION

1.1 INTRODUCTION AND SUMMARY

The overall objective of this program is to grow advanced multilayer heterojunction epitaxial structures suitable for photovoltaic detection in the 12 μm spectral region using molecular beam epitaxy (MBE) on optically transparent substrates. Investigations under the program include the growth of single epitaxial layers of HgCdTe by MBE, doped both n- and p-type using extrinsic dopants, and the successive growth of layers for forming double-layer p-n heterojunctions (DLHJs). The layers and the junctions are evaluated using a variety of diagnostic tools to determine chemical, electrical, and structural characteristics pertinent to IR detector performance.

Substantial progress has been made in several critical areas of the program. We have established a strong MBE capability for growing device quality HgCdTe layers required for IR detector fabrication. The MBE system has been systematically modified and state-of-the-art layers of HgCdTe with excellent control in composition and semiconductor properties have been grown. Some major highlights are:

- A breakthrough in p-type doping which led to the controlled growth of extrinsic p-type layers of HgCdTe doped with arsenic in the range of 10^{15} to 10^{18} cm^{-3} that remain p-type even after mercury anneal.
- Controlled n-type doping of HgCdTe(x=0.2) achieved by using indium in the range of 10^{16} to 10^{18} cm^{-3} with mobilities which ranged from $2x10^4$ to $8x10^3$ $cm^2/V \cdot s$.
- Excellent transport characteristics observed for the undoped HgCdTe layers (x=0.18) μ_e = $2.2x10^5$ cm^2 $V \cdot s$ at 10K for n=$2x10^{15}$ cm^{-3}.

- PC decay measurements with excess carrier lifetimes of 2 to 4 μs for As-doped p-type HgCdTe(x=0.3) and 500 to 650 ns for In-doped n-type HgCdTe(x=0.2); lifetimes are comparable to those observed in state-of-the-art liquid phase epitaxy (LPE) layers.

- Orientation effects on epitaxial layers of the ternary demonstrated; doping kinetics for (100) and (111) orientation are quite different and need to be optimized separately for detector processing.

- Initial double layer heterojunction structures fabricated using two approaches: in-situ MBE approach and the MBE-LPE hybrid approach. The p-n junction formation was demonstrated and several 8 mil by 9 mil diodes were fabricated. The i-v characteristics of these diodes were measured.

These results are extremely encouraging and clearly demonstrate that MBE is suitable for IR detector fabrication. The details of the technical approach tht we used, layer and structure characteristics, and suggestions for further optimization are discussed in the following sections.

1.2 APPROACH

First, we will develop procedures for MBE growth of undoped single layers of HgCdTe with composition appropriate for detection of 12 μm radiation and with intrinsic carrier concentration below 10^{15} cm^{-3} at 77K. Subsequently, we will develop procedures for MBE growth of single n-type (x=0.2) and p-type (x=0.3) layers of HgCdTe by the addition of extrinsic dopants such as indium and arsenic during growth. Control of carrier concentration is within the range of 10^{15} cm^{-3} to 10^{18} cm^{-3}. Our approach for junction formation is to grow a wide band gap p-type cap layer (x=0.3) on a narrow band gap n-type base layer (x=0.2), as shown in Figure 1, for backside illumination.

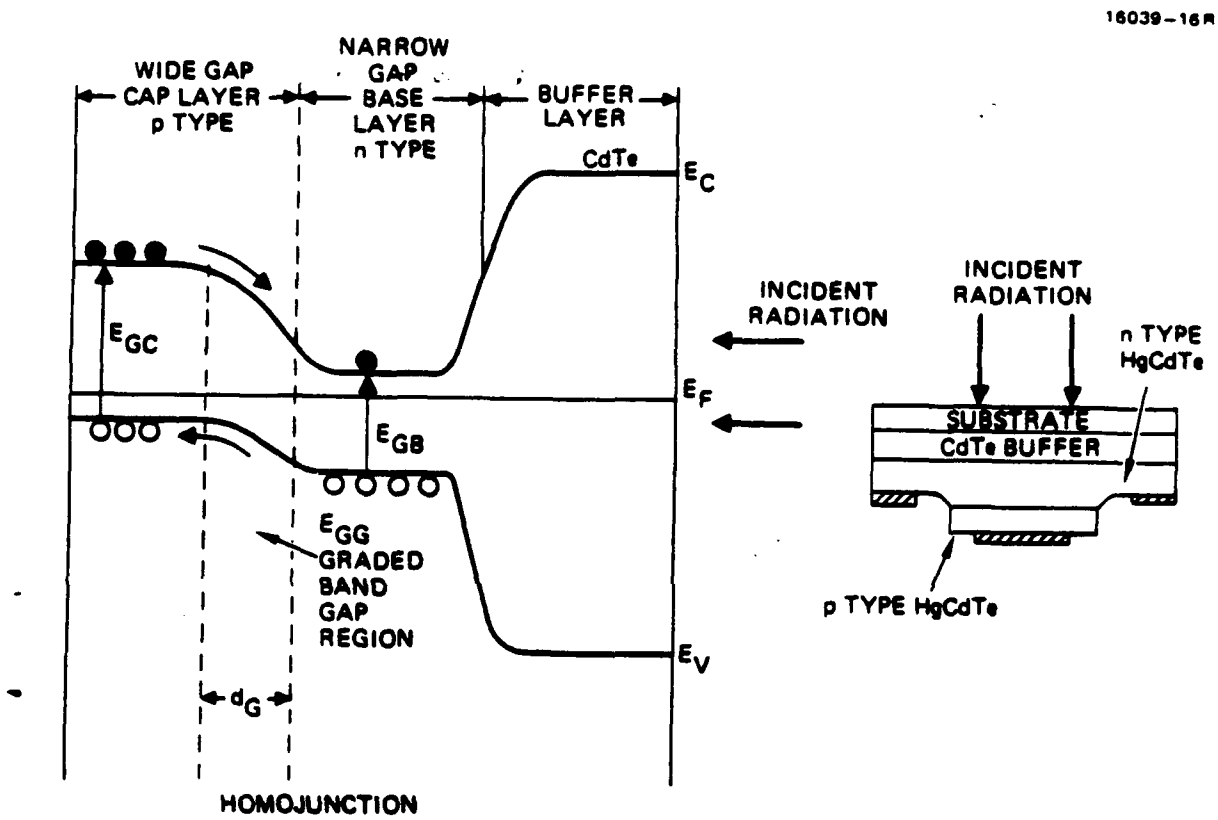

FIGURE 1. Double layer heterojunction structure and its band diagram.

SECTION 2

TECHNICAL PROGRESS

2.1 MBE FACILITIES

The MBE system used for this program is shown in Figure 2. It is a modified V80H MBE system from Vacuum Generators, Inc., dedicated to the growth of HgCdTe and related compounds, and includes several unique features specified by Hughes to improve the efficiency of the growth and analysis. The system consists of six interconnected chambers, including two preparation and entry chambers, an ESCALAB chamber, a buffer chamber, a transport chamber, and a chamber for growing mercury-based compounds.

In the chambers dedicated to growth activities, substrates can be baked out by high temperature heaters in the preparation chamber. This feature is particularly important for achieving intrinsic carrier concentrations below $1x10^{15}$ cm^{-3} at 77K. The buffer chamber is an important addition to our system compared with any other existing unit. It is a separately pumped, separately bakeable ultrahigh vacuum (UHV) chamber between the substrate preparation chamber, and the deposition chamber. Its primary functions are to control mercury spillover from the deposition chamber into the substrate preparation chamber, and to prevent contamination and doping of the substrate surface during outgassing in the growth preparation chamber.

The growth chamber has eight effusion cells, a dual mercury vapor source, and a port for IR or optical pyrometry. A DEC micro-PDP-11 computer is used to control effusion cell temperatures and shutters. Computer automation permits us to control all the cell and substrate manipulator functions necessary to grow the $Hg_{1-x}Cd_xTe$ alloys. The dual mercury vapor source allows us to load mercury without breaking vacuum and to change the partial pressures of mercury instantaneously to permit growth of alloys with different compositions.

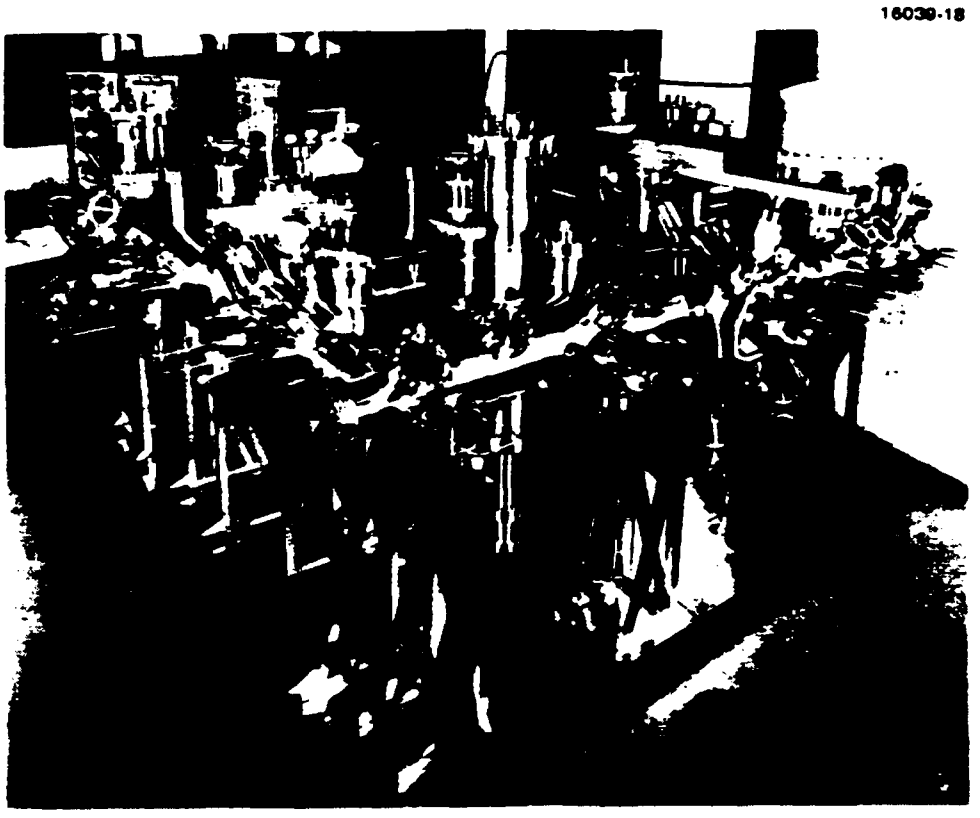

FIGURE 2. II-VI MBE growth facility at HRL.

Full beam monitoring facilities are available to monitor dynamic beam composition and intensity information during deposition. The monitoring system consists of an sxp 300 (1 to 300 amu) quadrupole mass spectrometer with a cross-beam ionization source and a monitoring ionization gauge. By tilting the sample manipulator drive, the ionization gauge can be sited in the position normally occupied by the substrate during growth. In this position, the beams from the individual source can be monitored and calibrated. The deposition chamber is also equipped with a reflection high energy electron diffraction (RHEED) system to provide structural information for substrate preparation monitoring and to aid in the control of crystal quality and growth rate.

In addition to the buffer chamber, our system is equipped with specific features unique to Hughes to ensure maximum up-time of the machine. Particular attention has been paid to the control of mercury in the system. Every chamber is equipped with custom-designed liquid nitrogen and cold trap assemblies and appropriate valving so that condensed mercury can be removed from the chamber, into the trap, and then through the high vacuum pumping area. In addition, these same traps permit changing the filaments in every titanium sublimator except for the huge sublimator in the deposition chamber without venting or baking the associated chamber or high vacuum pump. Every chamber in the system is capable of attaining pressures of 5×10^{-10} Torr or less and each chamber is equipped with a quadrupole residual gas analyzer to monitor mercury contamination.

Furthermore, the main deposition chamber includes important features to facilitate monitoring of mercury buildup and to hasten mercury recovery. For example, a special cold trap has been provided to collect mercury during the bakeout; when the liquid mercury collects in the trap, it can be removed without breaking vacuum. This is important to maximize the speed and efficiency of mercury removal during bakeout.

2.2 GROWTH PARAMETERS CONTROL

To grow high quality HgCdTe and DLHJ structures, the reproducible control of growth parameters is essential. While testing the reproducible control of our growth parameters for $Hg_{1-x}Cd_xTe$ alloy layers, we encountered two major problems: (1) ensuring the stability of CdTe and tellurium beam fluxes, and (2) attaining accurate measurement of the substrate surface temperature during growth. We have developed growth procedures to solve these problems. The first problem was alleviated by reducing the source heating rate to 0.2°C/s and by placing more tantalum foil at the front end of the crucibles as a heat shield. Using this technique, we obtained relatively stable beam fluxes (within ±5%) for both CdTe and tellurium sources. For the mercury flux, the stability achieved was within ±2%. We are also using a cracker cell for tellurium to obtain a more stable beam flux. In this program, we used these procedures to obtain stable fluxes of CdTe, tellurium, and mercury for the HgCdTe growth.

Substrate temperature measurement and control is more difficult, since the thermal characteristics of each substrate holder depend on the history of the deposition runs made on it. For example, the surface temperature of a CdTe-coated substrate holder can be 20°C higher than that of a HgTe-coated substrate holder for comparable temperatures at the back of the molybdenum substrate holder. The real surface temperature of a substrate holder is also affected by the morphology, composition, and thickness of the film deposited previously. In this program, we used a set of special molybdenum substrate holders with an optical finish (0.3 μm) to reduce the variation from holder to holder. In addition, a small piece of indium wire was mounted on the substrate holder, and its melting point was used as an indicator for the substrate surface temperature calibration during each MBE growth experiment.

2.3 SUBSTRATE PREPARATION

We used mainly CdTe(111) substrates and occasionally CdTe(100) substrates for comparison. These substrates were first degreased with triple solvents (trichloroethylene, methanol, and acetone) for about 30 min, then etched under 1/16% Br-methanol solution for about 60 s, and then rinsed thoroughly with methanol. The substrates were blown dry with dry nitrogen prior to mounting onto the substrate holder. The substrates were then mounted on a disk-shaped molybdenum holder with a carbon dag mixture, which provides both thermal and mechanical contact. The substrate holder was subsequently transferred through an entry chamber to the preparation chamber and baked at 150°C for several hours to remove water vapor and solvents. After this baking step, the holder was transferred through the buffer chamber to the growth chamber. The holder rotates at a speed of 60 rpm during growth for uniformity. Before MBE growth, the substrates were generally heat cleaned at 300°C for 15 min to remove surface oxides and contaminants. Growth rate was calibrated by measuring the thickness of a film grown simultaneously on a silicon substrate mounted on the sample holder. The thickness was measured by Dektak profilometry across a step created after growth by photolithographically etching off the HgCdTe on the silicon.

2.4 UNDOPED $Hg_{1-x}Cd_xTe$ MBE GROWTH AND CHARACTERIZATION

2.4.1 Optimization of CdTe and HgTe Growth

During the first few months of this program, we worked on fine tuning parameters for CdTe and HgTe growth in preparation for HgCdTe alloy growth. This optimization is essential for a high quality CdTe buffer layer growth, as well as for minimizing the mercury vacancies in the HgTe layer. The parameters studied included the source temperatures of CdTe, mercury and tellurium, and the substrate temperature. As a result of these

experiments, we improved the surface morphology and the single crystal quality of the epitaxial layers, as determined by scanning electron microscopy (SEM), reflectance high energy electron diffraction (RHEED), double crystal x-ray crystallography (DXRC), and Hall measurements. For example, we have grown CdTe epitaxial layers with double-crystal rocking curve half-widths less than 50 arcsec on CdTe substrates. Similarly, we have grown HgTe epitaxial layers that give rocking curve half-widths of <80 arcsec. Rocking curve half-widths can be further improved when higher quality CdTe substrates become available.

Table 1 lists some of the optimized growth conditions for high quality CdTe buffer and HgTe epitaxial layer growth. In general, we are able to grow high quality CdTe buffer layers in the temperature range of 230 to 300°C. Below 230°C, the quality of CdTe film degrades because of tellurium microprecipitates. The growth rate is about 1.5 μm/h with a CdTe source at 700°C and a pressure of 2×10^{-6} mbar.

By careful adjustment of the growth parameters and through study of the relative fluxes of the components necessary for orderly nucleation and growth of the HgTe, we have been able to reduce the flux ratio of mercury to tellurium to about 130, as listed in Table 1. The ratio compares with about 1000 used in

TABLE 1. Optimized Growth Conditions for CdTe Buffer Layer and HgTe Epitaxial Layer Growth.

C-8469-3

Source	Pressure (mbar)	Source Temperature (°C)
CdTe	2×10^{-6}	620
Te_2	1.3×10^{-6}	440
Hg	1.6×10^{-4}	125

most of the previous work. The reduction of the mercury flux by more than an order of magnitude is extremely significant in the reduction of materials deposition on the cryoshroud; it significantly reduces the downtime of the system for maintenance, and promotes a growth environment more compatible with the MBE techniques.

2.4.2 Optimization of Growth Temperature

We have also carried out HgTe growth as a function of growth temperature ranging from 163 to 183°C by using a fixed mercury pressure of 1.6×10^{-4} mbar and tellurium pressure of 1.3×10^{-6} mbar. This set of experiments was initiated to optimize the growth temperature in order to minimize the mercury vacancies in the layers. Figures 3(a) and 3(b) show carrier concentrations as a function of growth temperature for (111) and (100) orientations at 300K and 77K, respectively. Figures 4(a) and 4(b) show Hall mobilities as a function of growth temperature for (111) and (100) orientations at 300K and 77K, respectively. The results indicate that the HgTe has good electrical properties within the growth temperature range of 168 to 178°C. The growth rate under these conditions is about 1 μm/h. Above 178°C, the mercury vacancies dominate, so the normally expected n-type carriers are compensated. Below 168°C, the layer becomes polycrystalline. Studies by SEM indicate that the layers grown at 170°C give the best surface morphology. Accordingly, we chose 170°C as the growth temperature for most of our HgCdTe alloy studies.

2.4.3 $Hg_{1-x}Cd_xTe$ Alloy Growth: Control of X Value

Using the best experimental parameters derived from our studies, we have grown several excellent quality $Hg_{1-x}Cd_xTe$ alloys. For this program, we have made more than 100 runs to grow HgCdTe alloys, mostly using fixed fluxes of mercury (1.6×10^{-4} mbar), tellurium (1.3×10^{-6} mbar), and a fixed

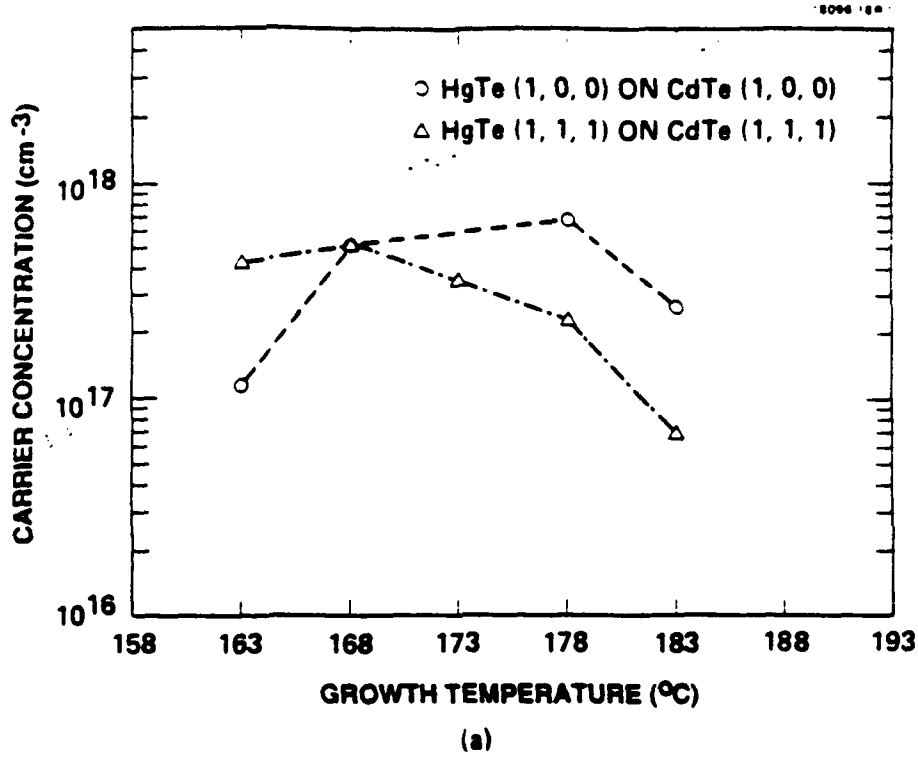

(a)

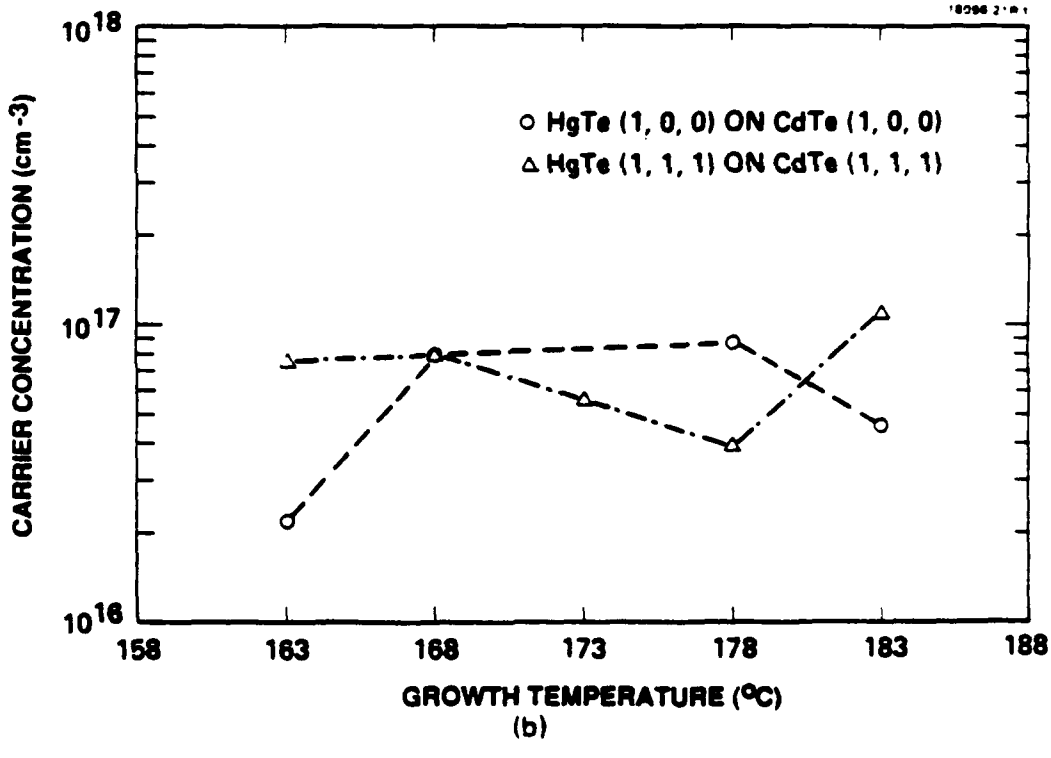

(b)

FIGURE 3. (a) Carrier concentrations of HgTe as a function of growth temperature determined by Hall measurements at 300K for both (111) and (100) orientations. (b) Carrier concentrations of HgTe as a function of growth temperature determined by Hall measurements at 77K for both (111) and (100) orientations.

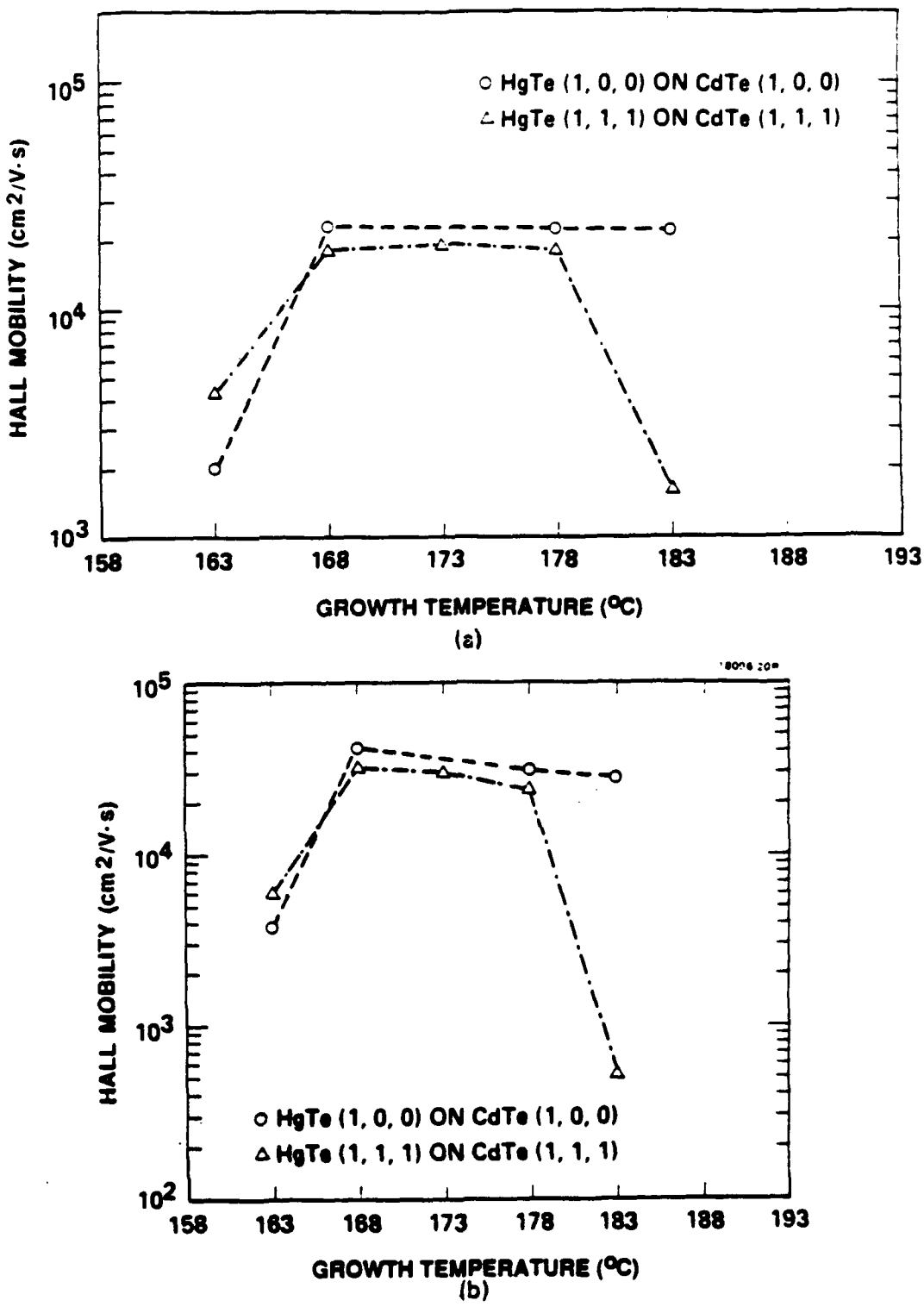

FIGURE 4. (a) Hall mobilities of HgTe as a function of growth temperature determined by Hall measurements at 300K for both (111) and (100) orientations. (b) Hall mobilities of HgTe as a function of growth temperature determined by Hall measurements at 77K for both (111) and (100) orientations.

substrate temperature (170°C). The X value of $Hg_{1-x}Cd_xTe$ ranged from 0.18 to 0.38, according to the CdTe source temperature, as shown in Table 2. The X values are determined by energy dispersive x-ray analysis and photoreflectance techniques. The results are in reasonable agreement. The growth rates of this set of samples are also listed for comparisons.

2.4.4 Characterization of MBE-Grown HgCdTe Layers

For DLHJ device applications, we have to optimize the HgCdTe layer quality from structural, chemical, optical, and electrical points of view. In this program, we use double-crystal x-ray rocking curve measurements to assess crystal quality, and use SEM to examine surface morphology. Secondary ion mass spectrometry (SIMS) is used to determine the quantities of unintentional and intentional dopant impurities in the layers. Infrared transmission and photoluminescence techniques are used to measure the cutoff wavelength and band gaps of the layers. Photoconductive decay measurements are carried out to try to understand the lifetime of the minority carriers. Hall effect measurements are carried out on every sample to determine the carrier concentrations and mobilities at 300K and 77K. Results obtained are given in the following sections.

2.4.4.1 Structure Characterization. Our SEM results indicate that the morphology of HgCdTe alloys grown on (100) substrates is better than that obtained on (111)B substrates for our growth parameters. These results suggest that the conditions for growth on the (100) and (111) planes are different and must be separately optimized. Double-crystal x-ray rocking curve data also show that HgCdTe layers grown on (100) substrates have better crystal quality (narrower half-width) than that obtained on (111)B substrates. For example, Figure 5 shows the double-crystal x-ray rocking curve half-width is about 105 arcsec on Sample MCT-79B, which was grown on a (100) CdTe substrate,

TABLE 2. Growth of $Hg_{1-x}Cd_xTe$: Control of X.

C-8469-4

Sample	CdTe °C	Pressure (mbar)	X Value	Growth Rate (μm/h)
MCT-75	635	4.2×10^{-7}	0.13	1.2
MCT-74	645	5.1×10^{-7}	0.16	1.2
MCT-73	655	6.3×10^{-7}	0.20	1.4
MCT-76	665	7.1×10^{-7}	0.25	1.4
MCT-77	675	9.6×10^{-7}	0.38	1.6

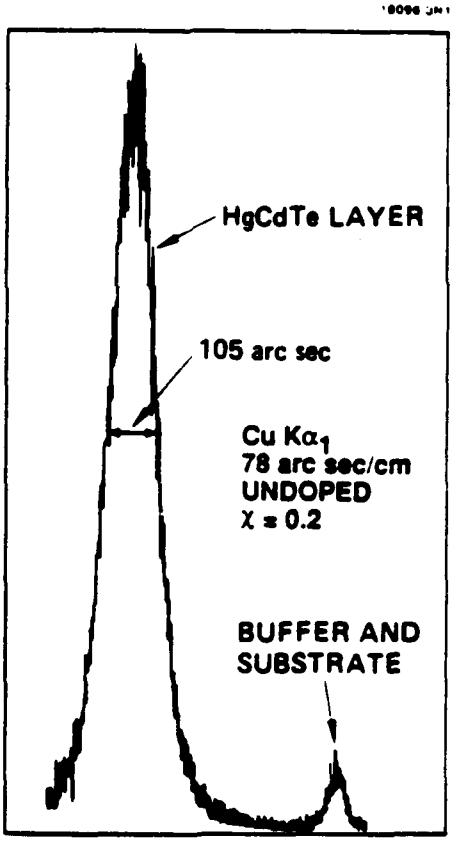

FIGURE 5. Double crystal x-ray rocking curve data for an MBE HgCdTe (x=0.2) layer showing the full width at half-maximum is 105 arcsec.

whereas (111)A had a half width of 145 arcsec. We have also grown HgCdTe(100) alloys with x-ray rocking curve half-width about 60 arcsec when the substrates are of high quality (less than 20 arcsec). Transmission electron microscopy (TEM) analysis confirms these results, and indicates that the defect density of CdTe epitaxial layers grown on (111)B substrates is at least two orders of magnitude higher than that of CdTe epitaxial layers grown on (100) substrates. These results may be partially due to the nonequilibrium MBE deposition process on polar versus nonpolar substrates. The number of stacking faults in epitaxial layers grown on polar substrate surfaces is higher than that in nonpolar substrate surfaces. The investigation of this aspect of MBE growth should be continued since specific orientations may be preferred either for device processing or for device characteristics.

2.4.4.2 Optical Characterization. Our optical characterization techniques for HgCdTe include IR photoluminescence and transmission and reflection as functions of temperature (from room temperature to liquid helium). These measurements give us information about the IR absorption properties of these materials as well as their band gaps.

To determine the cutoff (λ_{co}) wavelength of HgCdTe materials, we routinely perform IR transmission measurements on MBE-grown alloy layers in this program. Figures 6 and 7 show the IR transmission curve of sample MCT-50A&B at room temperature. This is an MBE-grown $Hg_{1-x}Cd_xTe$ alloy layer 4.5 μm thick with x=0.28. The result showed that this sample has a relatively sharp cutoff (λ_{co}) wavelength at 4.7 μm, indicating excellent compositional uniformity.

We have also observed IR photoluminescence signals from our MBE-grown HgCdTe alloy layers. The results were particularly interesting, since this was the first known measurement of IR photoluminescence of an MBE alloy sample. The sample had a

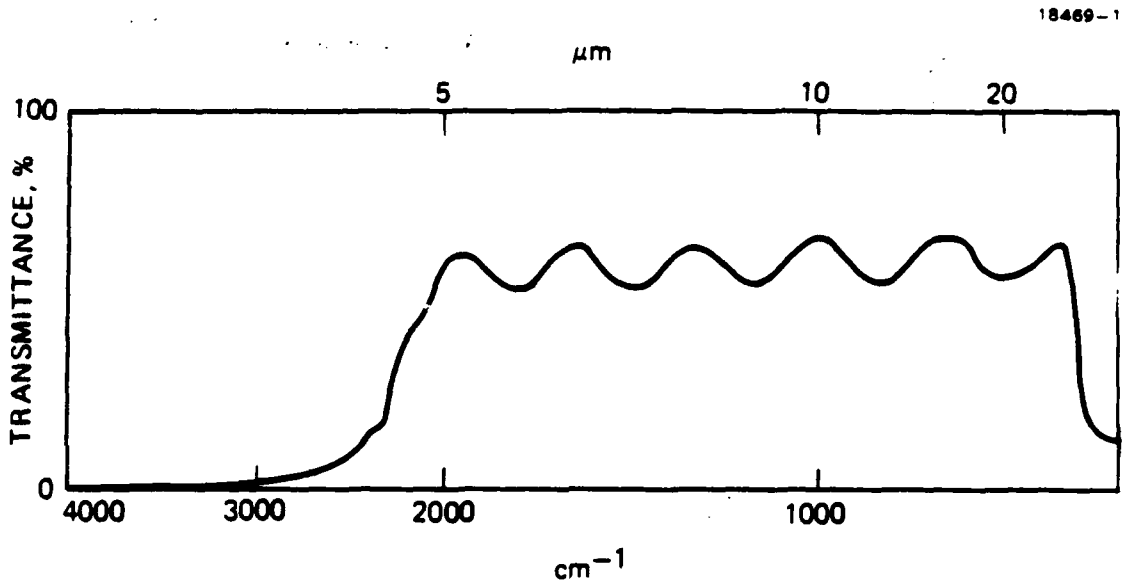

FIGURE 6. IR transmission data for an MBE HgCdTe layer grown on a CdTe (111) substrate showing the cutoff wavelength (4.7 μm).

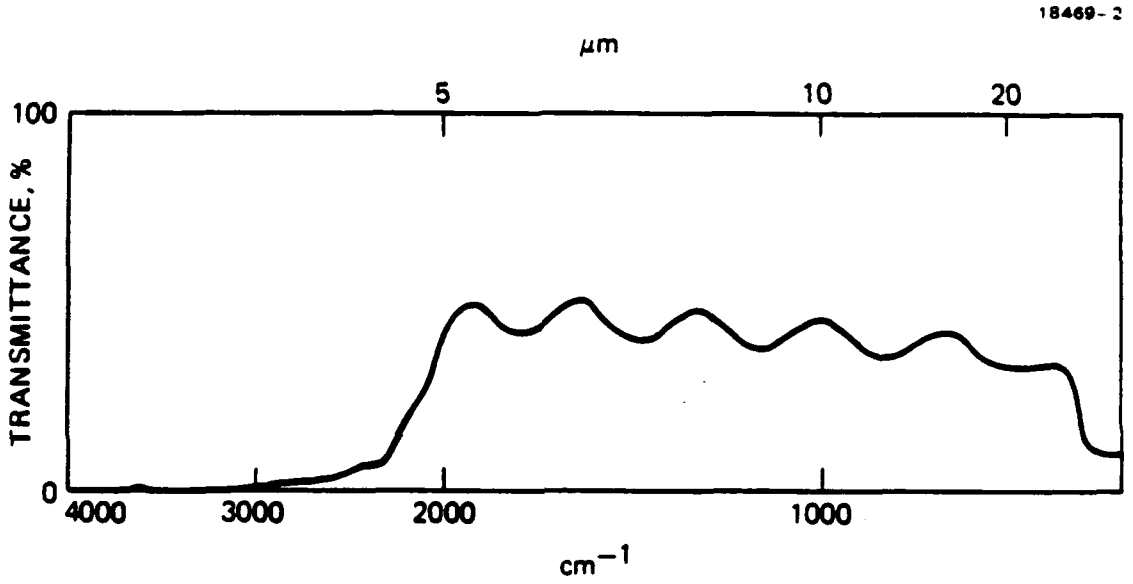

FIGURE 7. IR transmission data for an MBE HgCdTe layer grown on a CdTe (100) substrate showing the cutoff wavelength (4.8 μm).

single emission peak at 1225 cm^{-1} (8.2 μm) at 5K. The energy of peak position increased with increasing temperature, as expected, but the emission intensity weakened rapidly. The data suggest that the sample is of high quality. This technique can also be used to characterize the n-type and p-type layers and to compare them with undoped layers to determine the impurity energy levels of indium and arsenic in the HgCdTe band gap.

2.4.4.3 Carrier Lifetime Measurement. Minority carrier lifetime measurements are routinely performed on LPE layers at the Hughes Santa Barbara Research Center (SBRC) by photoconductive decay technique using a 0.63 μm HeNe laser with an acousto-optic modulator.

We have performed carrier lifetime measurements on several MBE-grown HgCdTe layers. The samples generally exhibited well-behaved (single-exponential) photoconductive decay behavior at room temperature. The 300K lifetimes ranged from 30 to 40 ns for long wavelength (LWIR) ($x \approx 0.22$) material, and from 400 to 500 ns for medium wavelength infrared (MWIR) ($x \approx 0.28$) material. These values are consistent with measured results for comparable LPE-grown HgCdTe layers. However, for temperatures below about 200K, the majority of the samples exhibited multi-exponential decay behavior. The decay times were often as high as 200 μs. The long decay times and multi-exponential characteristics suggest that trapping effects are dominating the photoconductive decay measurements. Under these conditions, the decay time is not believed to be indicative of the minority carrier lifetime. The trapping effects are suspected to be the result of a material inhomogeneity at the interface region between the epitaxial layer and the substrate. These effects are occasionally observed in LPE samples, but are believed to be more extensive in the MBE samples because of the reduced thicknesses of the layers.

Sample MCT-38A exhibited the single-exponential behavior shown in Figure 8 over the entire temperature range of 80 to 300K. The lifetime of this sample was approximately 1 μs at 80K. This value is comparable with that observed for similar low-doped LPE material. The minority carrier lifetimes of n-type and p-type HgCdTe layers have been measured and are discussed in Section 2.5, Chemical Doping of HgCdTe.

2.4.4.4 Electrical Characterization. Hall measurements on HgCdTe epitaxial material are complicated by mixed conduction of electrons and holes, arising both from the narrow band gap and from layer stratification effects. Since the presence of mixed conduction can lead to an erroneous determination of carrier concentration, detection of mixed conduction and measurement correction is important. Intrinsic electron conduction will dominate above ~100K because of the narrow band gap of LWIR materials. Hence, all Hall measurements must include a low-temperature region, extending down to 77K or lower.

Detection of the presence of a stratified layer structure (n-skin on p-bulk, for example) can be made either with variable field or with variable temperature measurements. Variable field measurements at 77K require less time than variable temperature measurements, but do not provide information concerning freeze-out and the activation energies of p-type dopants.

The variable-field technique relies on the difference in cyclotron frequency ω_c of electrons and holes at a given magnetic field in order to detect mixed conduction. As the field increases, the transition from low field ($\omega_c\tau<1$) to high field ($\omega_c\tau>1$) causes a decrease in the Hall coefficient. The field strengths at which these transitions occur are much lower for electrons than holes in HgCdTe, and are proportional to the differences in effective mass. The Hall coefficient plot as a function of magnetic field will exhibit plateaus or sign changes, depending on the ratio of the carrier concentrations.

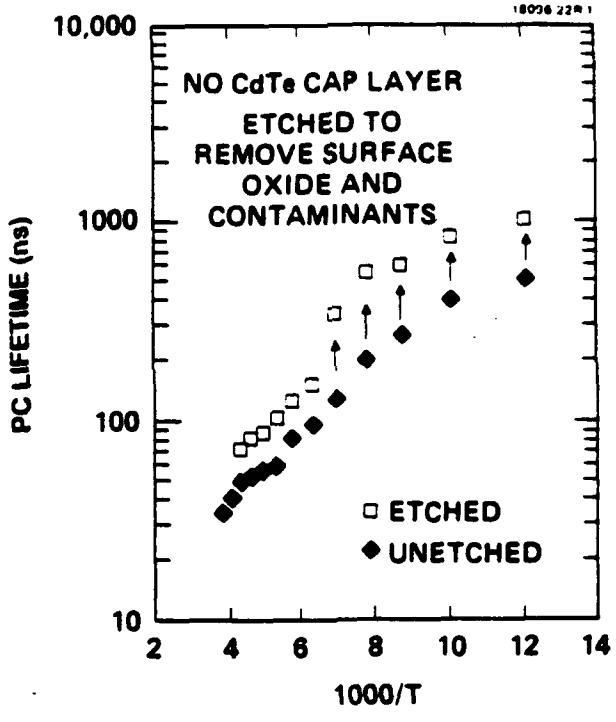

FIGURE 8. Photoconductive decay lifetime as a function of temperature for an MBE-grown HgCdTe layer (x=0.2).

The variable-temperature Hall measurement depends on the difference in activation energies of electrons and holes and their resulting freeze-out characteristics. As holes freeze out at low temperatures, it is possible to detect small concentrations of electrons that do not freeze out. Typical experimental variable-temperature data are shown in Figures 9, 10, 11 and 12 for x=0.16 to 0.28 HgCdTe alloy layers. Figure 9 shows the carrier concentration and mobility as a function of temperature for sample MCT-14B. In this case, the carrier concentration at 300K is $4x10^{16}$ cm^{-3}, and decreases to $7x10^{14}$ cm^{-3} at 10K. The mobility of this sample was previously measured to be 92,000 $cm^2/V\cdot s$ at 77K, which is a factor of 2 higher than these data. This is probably due to the surface conversion causing the decrease of mobility. Variations of electrical properties of a similar nature have been observed in prior work as a function of exposure to various ambients. An understanding of this effect is especially significant to the controlled intentional doping of the ternary, particularly at low doping levels. We are now depositing a CdTe cap layer about 2000 to 3000 Å on top of the $Hg_{1-x}Cd_xTe$ layers to avoid surface conversion and/or reactions at the HgCdTe surface.

An experiment (MCT-50) was made to grow an x=0.28 $Hg_{1-x}Cd_xTe$ alloy layer with thickness >4 μm to increase the total optical absorption in the layer. Cross-sectional SEM analysis indicates that sample MCT-50 has an epitaxial layer 4.5 μm thick with excellent morphology. Van der Pauw measurement, shown in Figure 10, indicates that the epitaxial layer was n-type ($5x10^{16}$ cm^{-3}) with a Hall mobility of $6.5x10^3$ cm^2 $V\cdot s$ at room temperature, and was n-type ($1x10^{14}$ cm^{-3}) with a Hall mobility of $1x10^4 cm^2$ $V\cdot s$ at 77K.

Another experiment (MCT-58) was made to grow an x=0.16 layer with thickness 7 μm. Van der Pauw Hall measurements (Figure 11) show that the epitaxial layer was n-type ($1x10^{17}$ cm^{-3}) with a Hall mobility of $8x10^3$ $cm^2/V\cdot s$ at room

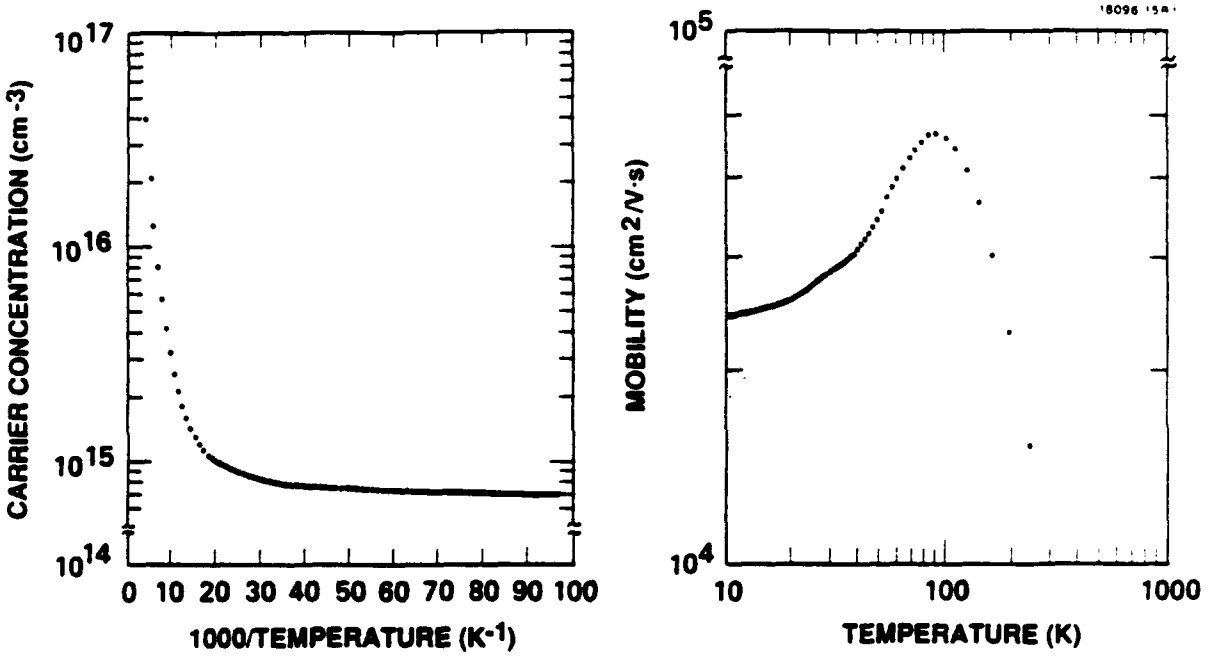

FIGURE 9. Hall data (carrier concentration and mobility) as a function of temperature for an MBE-grown HgCdTe (x=0.22) layer.

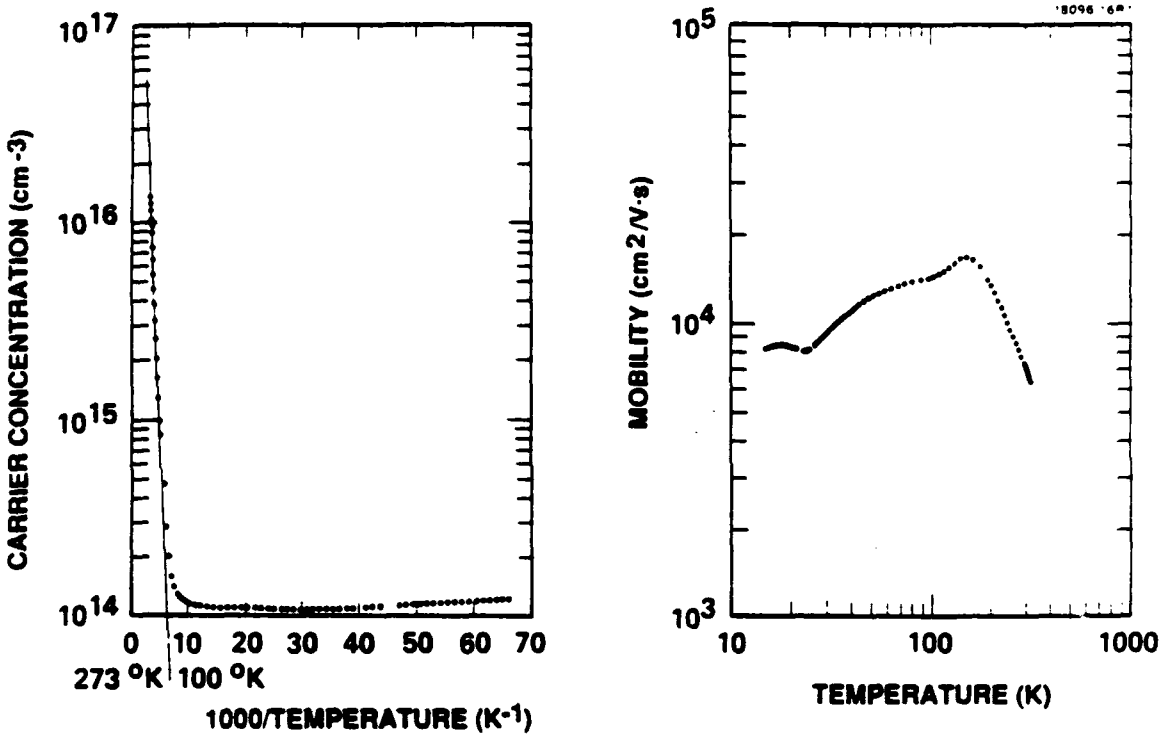

FIGURE 10. Hall data (carrier concentration and mobility) as a function of temperature for an MBE-grown HgCdTe (x=0.28) layer.

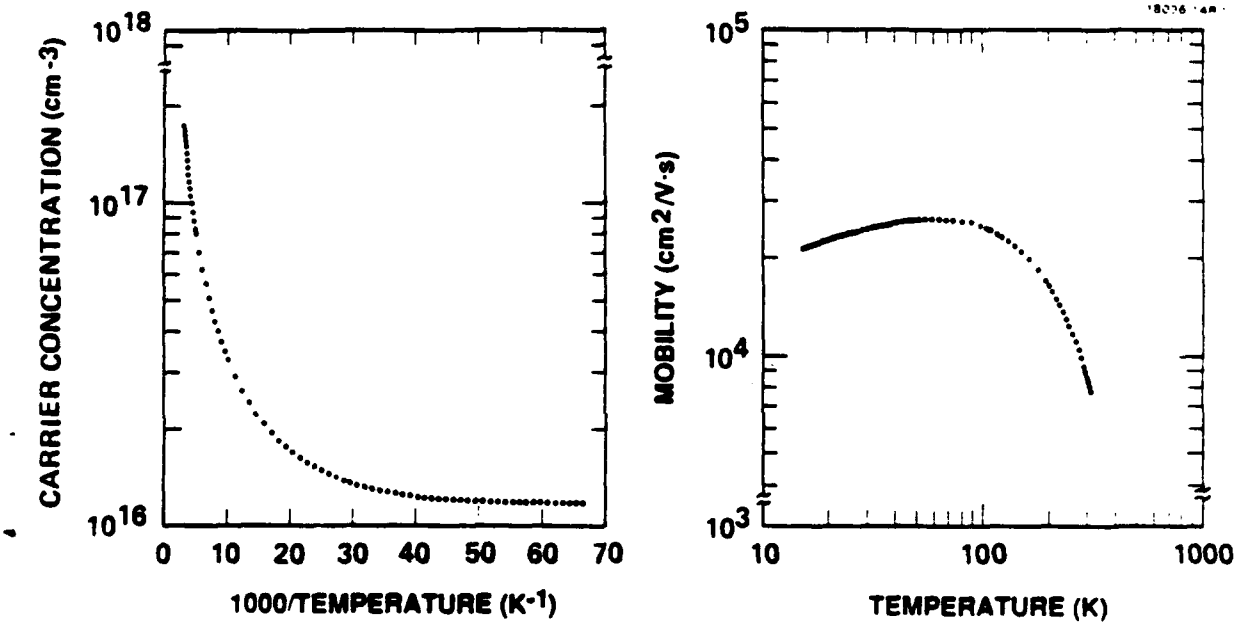

FIGURE 11. Hall data (carrier concentration and mobility) as a function of temperature for an MBE-grown HgCdTe (x=0.16) layer.

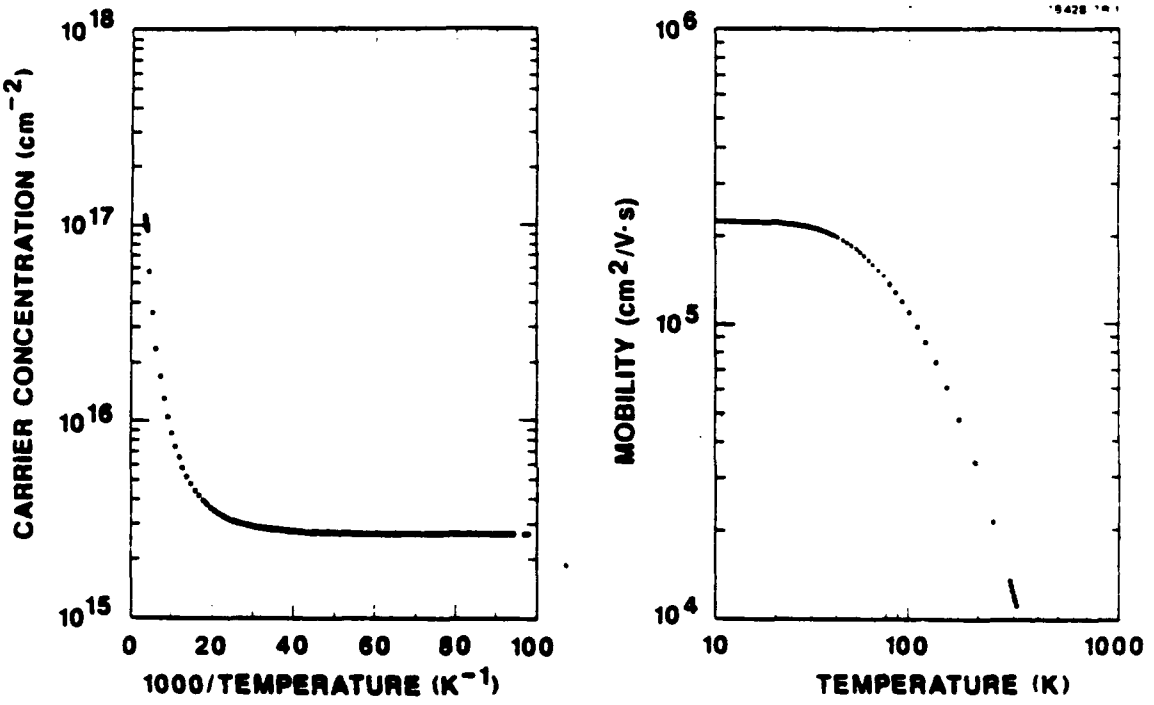

FIGURE 12. Hall data (carrier concentration and mobility) as a function of temperature for an MBE-grown HgCdTe (x=0.19) layer.

temperature and was n-type ($1x10^{16}/cm^3$) with a Hall mobility of $2x10^4$ $cm^2/V \cdot s$ at 77K.

Figure 12 shows the carrier concentration and mobility as a function of temperature for an alloy layer (x=0.19) with a 3000-Å CdTe cap layer. The data indicate that the carrier concentration at 300K is $1x10^{17}$ cm^{-3}, and decreases to $2.5x10^{15}$ cm^{-3} at 10K. The mobility increases with increasing temperature to a maximum value of 225,000 $cm^2/V \cdot s$ at about 10K. These data suggest that the undoped HgCdTe layers are of excellent quality.

Figure 13 is a plot of theoretical intrinsic carrier concentration as a function of temperature for different alloy compositions. This plot indicates that the intrinsic carrier concentrations are about $6.5x10^{15}$, $3x10^{14}$, and $<10^{16}$ cm^{-3} for x=0.15, 0.2, and 0.3, respectively. As shown above, our background doping ranges from 10^{16} cm^{-3} to 10^{14} cm^{-3} for x=0.16 and x=0.28 HgCdTe alloys are close to those values. We believe that the background doping can be decreased by 1 order of magnitude by baking the whole MBE system at 200°C more regularly. The low level of background doping is essential for controlled intentional chemical doping of HgCdTe especially at low x values.

2.5 CHEMICAL DOPING OF HgCdTe

2.5.1 Major Challenges

Chemical doping is one of the key elements in the development of advanced semiconductor devices. To produce heterostructure detectors with HgCdTe epitaxial layers, it is essential to understand and control dopant behavior. Intentional doping is usually necessary to produce well-behaved and stable junctions for photovoltaic devices. Although it is possible to use stoichiometric annealing methods[1,2] to control the charge carriers associated with native defects, such as mercury vacancies, this approach does not ensure the stability and repeatability required for device structures.

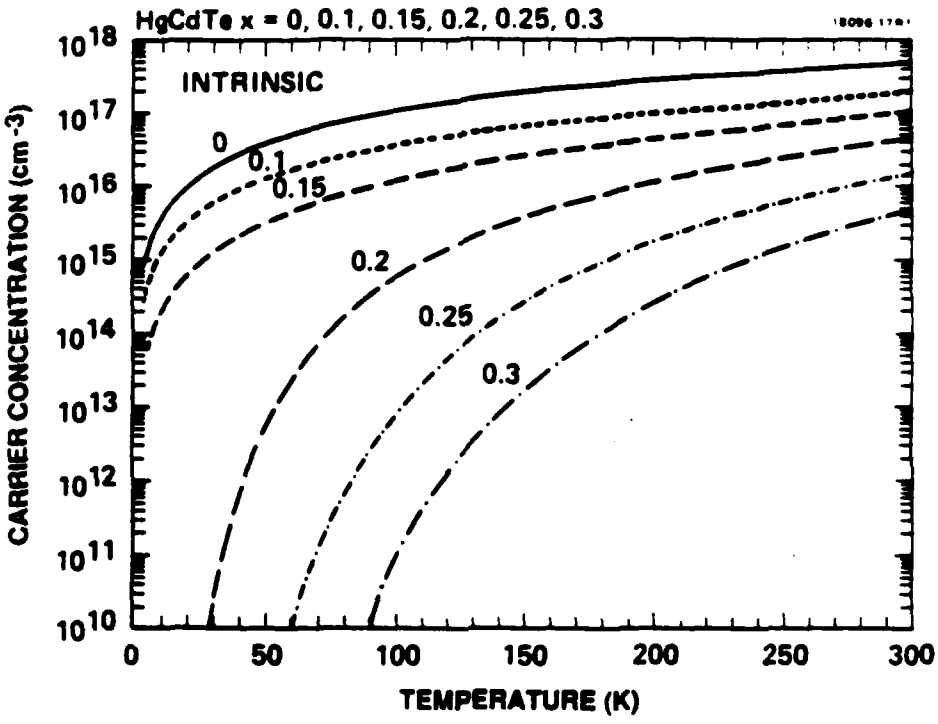

FIGURE 13. Theoretical intrinsic carrier of $Hg_{1-x}Cd_xTe$ as a function of temperature for different composition.

Although MBE has been used for nearly 15 years to synthesize a variety of unique semiconductor structures,[3] its use for the growth of HgCdTe films is relatively new. Over the past two years, major progress has been made in growing high quality HgCdTe alloy layers, as well as HgTe/HgCdTe superlattices, in a number of universities and industrial laboratories.[4] However, no conclusive evidence of reproducible chemical doping of both n and p type in HgCdTe has yet been achieved by MBE.

One of the most significant problems in MBE of HgCdTe is that the sticking coefficient of mercury is both low (on the order of 10^{-3}) and highly dependent on substrate orientation and temperature. Lowering or raising the substrate temperature[5] by a few degrees kelvin can change the carrier concentration in an epitaxial layer from p-type to n-type. The chemical doping issue is greatly complicated in the HgCdTe compounds by their proclivity for vacancy doping, caused by nonstoichiometry, and by the fact that IR detectors need precise control of doping in the 10^{15} cm^{-3} level. It has been widely accepted that excess tellurium leads to microprecipitation and is accommodated in the $Hg_{1-x}Cd_xTe$ lattice through the formation of metal (Hg-Cd) vacancies acting as doubly ionized acceptors.[6]

Recently, controlled substitutional doping of CdTe was demonstrated by the North Carolina State University group with a new growth technique, photo-assisted MBE.[7,8,15] They used an argon ion laser operating with broad-band blue-green optics (488.0 to 528.7 nm) as an illumination source, and achieved n-type doping with indium in the range of $7x10^{15}$ cm^{-3} to $6x10^{17}$ cm^{-3}, and p-type doping with antimony at $5x10^{16}$ cm^{-3}. The mechanisms of the photo-assisted MBE process are not well understood. For instance, it is believed that the argon ion laser generated tellurium vacancies are occupied by antimony dopant atoms; this assumption is based on C.J. Summers' observation that the activation energy for desorption of

tellurium atoms is only 1.95 eV.[9] There is, however, no comparable interpretation for n-type doping. In addition, the photo-assisted MBE process does not seem to apply to HgCdTe since they were not able to grow p-type antimony-doped HgCdTe alloy layers; n-type antimony-doped HgCdTe alloy layers were grown instead.[10]

Successful n-type doping of HgCdTe layers with indium during growth by conventional MBE was reported by the group at the University of Illinois at Chicago.[11,12] The indium concentration is found to increase with the indium flux to a level approaching 10^{18} cm^{-3}. However, they found that indium is not singly ionized, precipitates as In_2Te_3, and has memory effects in the growth chamber.[10,11] This phenomenon would make the growth of a double layer heterostructure, involving successive n- and p-type layers difficult. The memory effect must be further studied to determine whether either machine design or a more careful choice of dopant species could reduce the problem. They also found that the column V elements arsenic and antimony, and the column IV element silicon act as n-type dopants in HgCdTe when they are incorporated during the MBE process. The research group concluded that these impurities interact preferentially with the cation site and are self-compensated, since the doping concentrations remain low and impurity scattering limits the mobility at low temperature. Lithium[10,11] and silver[13] have been used as p-type dopants, substituting for the cation. Unfortunately, these are fast diffusing acceptors, according to Johnson and Schmit,[14] making their control difficult. The problem is especially aggravated with the narrow band gap HgCdTe alloy, because the doping levels in both layers must be lower than $1x10^{16}$ cm^{-3} and preferably as low as $1x10^{15}$ cm^{-3}, in the base layer.

In summary, the literatures survey indicated that several problems needed to be solved in developing double layer heterojunction detectors by MBE: (1) minimize the mercury and

cadmium vacancies, (2) reduce tellurium microprecipitates, (3) eliminate unwanted impurities in the system, (4) enhance the mercury sticking coefficient, and, most importantly, (5) realize growth conditions in which Group V elements can preferentially substitute in the tellurium sublattice to obtain p-type doping.

2.5.2 Antimony Doping: Growth and Characterization

We have carried out a series of experiments to grow HgCdTe alloys doped with antimony. Our antimony source was a special cracker cell designed for the generation of dimers from such Group V sources as arsenic and antimony; the cell is also used for the generation of monomers from dimers, such as tellurium. The cracker cell consists of two distinct temperature controlled heater zones. The first zone has a standard effusion cell configuration and is used for the controlled evaporation of the antimony source (generally occurring in the tetramer form). The evaporated species are then channeled into a second heater zone, in which they undergo multiple collisions at elevated temperature. This high temperature region induces the dissociation of antimony to the dimer species. By setting the first and second temperature zones at 250 and 500°C, respectively, we obtained an antimony beam pressure of 5×10^{-8} mbar. Initial experiments were made to grow $Hg_{1-x}Cd_xTe$ alloy layers at 170°C on CdTe(111) substrates with and without antimony dopant (MCT-36 and MCT-37). In these experiments, we deposited a 1000 Å cap layer of CdTe on top of $Hg_{1-x}Cd_xTe$ alloy layers as passivation films to allow optical and electrical measurements. The room temperature IR transmission measurements on MCT-36 and MCT-37 show a cutoff frequency of 4 to 5 μm. Hall measurements on sample MCT-37 (with antimony doping) indicated that this sample was n-type at room temperature with carrier concentration of 1.9×10^{16} cm^{-3}, but it became p-type at 77K with a carrier concentration of 3×10^{15} cm^{-3} (see Table 3).

TABLE 3. Hall Data at 300K and 77K for the Sample MCT-37 (Doped with Sb) as Grown and After Hg Annealing.

C18469-5

Sample	Carrier Concentration (/cm^3)		Mobility (cm^2/V•s)	
	300K	77K	300K	77K
As Grown	-1.9x10^{16}	3.05x10^{15} (p-type)	-7.02x10^3	1.37x10^2
After Hg Annealing	-2x10^{16}	-5x10^{15} (n-type)	-6x10^3	-1.5x10^4

A major problem encountered during these experiments was the instability of the antimony beam flux. The problem apparently occurs because the middle region between the first and second heated zone of the cracker cell has insufficient heat shields; as a result, antimony condenses and clogs the orifice located in this region. Extra heat shields (tantalum foil) were added to solve the problem, and the pressure versus temperature calibration curve was completed. This calibration curve covers a pressure range of ~1x10^{-10} to 5x10^{-9} mbar over a temperature range of 250/550°C to 350/750°C for the first and the second heated zones, respectively. We also found that water cooling is necessary for the cracker cells to allow independent temperature control of the first and second heated zones.

SIMS analysis on sample MCT-37 (shown in Figure 14) indicated that antimony was incorporated in the layer with a concentration of 2x10^{17} cm^{-3}. More experiments (MCT-62 and MCT-63) were carried out to test the reproducible control over our growth parameters for antimony-doped HgCdTe. We found that the 5x10^{-10} mbar of antimony flux significantly reduced the perturbation of the single-crystal HgCdTe alloy growth.

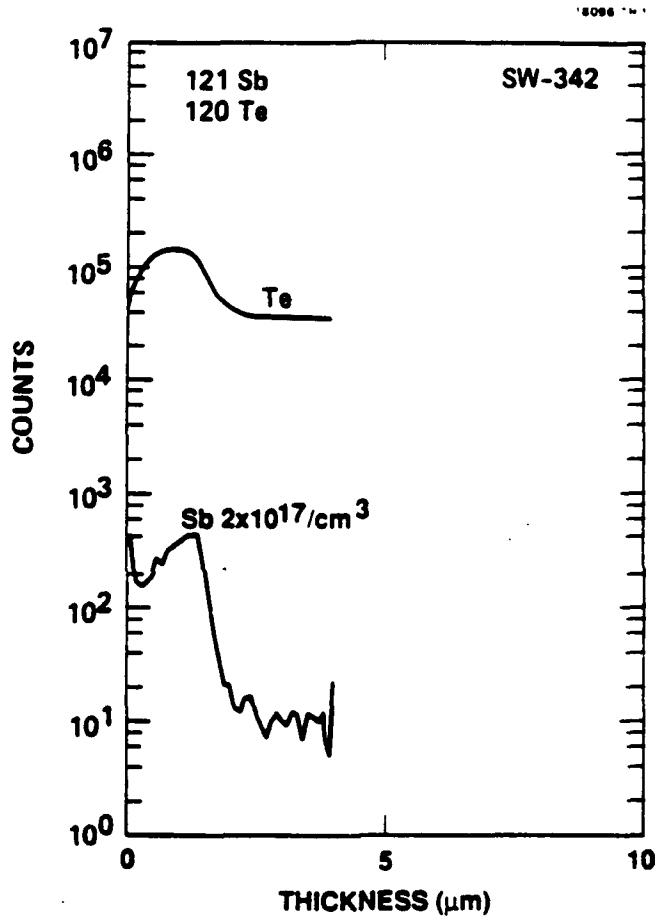

FIGURE 14. SIMS profile of an MBE-grown HgCdTe layer showing the doping concentration of antimony is $2x10^{17}/cm^3$.

2.5.3 Saturated Mercury Vapor Annealing

To confirm the p-type doping (antimony), we carried out saturated mercury vapor annealing experiments. In these experiments, several undoped and antimony-doped MBE-grown HgCdTe alloy layers were annealed under the saturated mercury vapor at 250°C for several hours at SBRC. If the antimony-doped samples stay p-type, it would prove that true p-type chemical doping was achieved.

Hall measurements (shown in Table 3) on these annealed samples indicated they were n-type at 77K. For instance, the sample MCT-37 (antimony-doped, before annealing) is p-type with a carrier concentration of $3x10^{15}$ cm^{-3} at 77K, and changed to n-type with a carrier concentration of $5x10^{15}/cm^3$. Table 4 also lists the Hall data for samples MCT-62A (undoped) and MCT-63A (antimony-doped) before and after annealing. The results indicate that the undoped sample was n-type before and after annealing, but that the antimony-doped sample changed from p-type to n-type after annealing. A comparison of these data and previous data on MCT-37 may be explained if antimony is amphoteric, and the balance under our conditions of experiment favors the cation sites leading to a net n-type doping. Thus the challenge is to find conditions which would direct antimony to the anion sites preferentially. Antimony doping by a cracker cell alone is apparently not sufficient to grow p-type alloy layers. We believe that it is important to minimize mercury vacancies in the materials in order to have group V elements occupy the anion sites. Therefore, a cracker cell was used to generate atomic tellurium for the growth of HgCdTe, assuming that the sticking coefficient of mercury will enhance in the presence of atomic tellurium and hence reducing mercury vacancies. Arsenic doping results using this approach are described in detail in Section 2.5.5.

TABLE 4. Hall Data at 300K and 77K for Samples MCT-62A (Undoped) and MCT-63A (Sb Doped), as Grown and After Hg Annealing.

C18469-6

	Sample	Carrier Concentration, ($/cm^3$)		Mobility ($cm^2/V \cdot s$)	
		300K	77K	300K	77K
Undoped	MCT-62A Before	n-Type $-3\ 4x10^{16}$	n-Type $-3x10^{15}$	$-8.5x10^3$	$-4.6x10^4$
	MCT-62A After	$-1.4x10^{17}$	$-2.5x10^{16}$	$-8.5x10^3$	$-2.6x10^4$
Sb Doped	MCT-63A Before	p-Type $1.2x10^{18}$	p-Type $1x10^{18}$	64	160
	MCT-63A After	n-Type $-6.2x10^{16}$	n-Type $-3.6x10^{16}$	$-4.8x10^3$	$-7x10^3$

2.5.4 Silver Doping

We grew several HgCdTe (x=0.3) alloy layers doped with silver. Silver is supposed to substitute for mercury or cadmium. Samples MCT-48 and MCT-49 were doped with silver with a beam flux of $5x10^{-9}$ and $5x10^{-10}$ mbar, respectively. Hall data (shown in Table 5) indicate that these samples were p-type at 300K and 77K. The carrier concentration ranged from $5x10^{17}$ cm^{-3} to $5x10^{18}$ cm^{-3}, with the highest mobility at 416 $cm^2/V \cdot s$. Stability of silver in $Hg_{1-x}Cd_xTe$ is somewhat in doubt, as discussed earlier. Therefore, the group I elements will not be used until we are convinced that Group V elements such as arsenic and/or antimony cannot be used to substitute in the tellurium sublattice.

2.5.5 Arsenic Doping: A Breakthrough

As discussed previously, the technical challenge for MBE growth of p-type HgCdTe is to find conditions in which Group V

TABLE 5. Hall Data at 300K and 77K for Samples MCT-48 and MCT-49 (Both Undoped with Ag).

C18469-7

Sample	Carrier Concentration (/cm^3)		Mobility (cm^2/V•s)	
	300K	77K	300K	77K
MCT-48A	4.02×10^{17}	1.29×10^{17}	3.95×10^{1}	6.89×10^{1}
MCT 48A′	5.27×10^{18}	2.83×10^{17}	1.12×10^{1}	8.00×10^{1}
MCT-48B (x = 0.31)	5.70×10^{18}	5.05×10^{18}	8.34×10^{1}	1.66×10^{2}
MCT-49A	5.71×10^{17}	3.69×10^{17}	6.45×10^{1}	1.39×10^{2}
MCT-49A′	5.72×10^{17}	3.68×10^{17}	6.74×10^{1}	1.61×10^{2}
MCT-49B (x = 0.28)	-4.19×10^{15}	2.11×10^{16}	-4.62×10^{3}	4.16×10^{2}

A = CdTe (111), A′ = CdZnTe (111), B = CdTe (100)

elements, such as arsenic, can preferentially substitute in the tellurium sublattice. To achieve this, we are using atomic tellurium produced from a cracker cell to reduce tellurium microprecipitates, to minimize the mercury and cadmium vacancies, and to enhance the mercury sticking coefficient during the growth of arsenic-doped HgCdTe alloy layers.

Using all these improvements, we initially tried to grow As doped HgCdTe layers using As as the dopant source. In our experiments we could not obtain controlled p-type doping in the layers grown. In parallel, we worked on p-type doping on our IR&D project using a variety of novel approaches. On approach has enabled us to obtain successful control over the p-type doping in the ternary material. As we had agreed in our proposal to make the results of our IR&D project available to the present contract, we have reported our results on As doping in our monthly reports and are discussing them below.

A series of growth runs was carried out to grow HgCdTe with and without arsenic doping. Samples grown were annealed and characterized electrically by Hall effect measurements. Table 6 summarizes the results obtained for samples MCT-86A and B, and MCT-87A and B. Samples MCT-86A and MCT-86B are undoped, and samples MCT-87A and MCT-87B are doped with arsenic at a flux of $1x10^{-9}$ mbar. The "A" denotes (111) orientation and the "B" denotes (100) orientation. The data indicate that the sample 87A is p-type with a carrier concentration of $6.7x10^{18}$ cm^{-3} and a Hall mobility of 61 $cm^2/V \cdot s$ at 77K. It appears that extrinsically arsenic-doped p-type HgCdTe is obtained, since the sample remains p-type after annealing under mercury ambient. Comparison of samples MCT-86A and B before and after annealing suggests that the mercury and/or cadmium vacancies are on the order of 10^{16} cm^{-3}. Sample MCT-87B was grown simultaneously with sample MCT-87A, and exhibited n-type behavior before and after annealing. Thus, we conclude that the doping kinetics for (100) and (111) orientation are quite different and need to be optimized separately.

To test the reproducibility of p-type HgCdTe growth on (111) orientation, we used growth conditions similar to those of MCT-87 to grow a series of samples doped with arsenic. The composition of these samples was approximately x=0.3, according to IR transmission measurements. Several samples were annealed and characterized by Hall measurements. Table 7 summarizes the results obtained for samples MCT-92A and MCT-92B before and after annealing. The data indicate that the as-grown sample MCT-92A is p-type with a carrier concentration of $5.8x10^{18}$ cm^{-3}, and a Hall mobility of 76 $cm^2/V \cdot s$ at 77K. After annealing under mercury ambient, the sample remains p-type. Thus we conclude that extrinsically arsenic-doped p-type HgCdTe alloy layers grown on (111) substrates seem to be reproducible. However, the HgCdTe alloy layers grown on (100) substrates in the same growth run give rise to n-type layers before and after annealing, as sample MCT-87B.

TABLE 6. Hall Data at 300K and 77K for Samples MCT-86 (Undoped) and MCT-87 (As Doped) as Grown and After Hg Annealing.

C18469-8

Sample	Annealing	Carrier Concentration (/cm^3)		Mobility (cm^2/V•s)		As Doping
		300K	77K	300K	77K	
MCT-86A	Before	-2.7×10^{16}	-1.4×10^{16}	4.4×10^{2}	1.4×10^{2}	No
	After	-1.0×10^{17}	-8.1×10^{16}	9.5×10^{2}	4.4×10^{2}	No
MCT-86B	Before	-1.7×10^{16}	-9.0×10^{15}	6.1×10^{3}	2.3×10^{4}	No
	After	-1.4×10^{17}	-9.5×10^{16}	3.4×10^{3}	1.3×10^{4}	No
MCT-87A	Before	$+6.7\times10^{18}$	$+6.7\times10^{18}$	4.3×10^{1}	6.1×10^{1}	Yes
	After	$+1.2\times10^{18}$	$+9.9\times10^{17}$	4.1×10^{1}	6.2×10^{1}	Yes
MCT-87B	Before	-2.8×10^{16}	—	2.9×10^{3}	—	Yes
	After	-5.8×10^{16}	-4×10^{16}	4.8×10^{3}	1.9×10^{4}	Yes

TABLE 7. Hall Data at 300K and 77K for Samples 92A and 92B (Both Doped with As) as Grown and After Hg Annealing.

Sample	Annealing	Carrier Concentration, (/cm^3)		Mobility (cm^2/V•s)		As Doping
		300K	77K	300K	77K	
92A	Before	5.3×10^{18}	5.8×10^{18}	53	76	Yes
	After	2×10^{18}	2×10^{18}	28	43	Yes
92B	Before	-3.3×10^{16}	-1.2×10^{16}	-6.8×10^{3}	-2.2×10^{4}	Yes
	After	-3.3×10^{16}	-1.4×10^{16}	-6×10^{3}	-1.9×10^{4}	Yes

A series of experiments was carried out to investigate the doping range of the growth of p-type HgCdTe alloys on (111) substrates. The results indicated that we were able to grow p-type HgCdTe (x=0.3) layers with a carrier concentration of 10^{15} to 10^{16} cm^{-3}. Table 8 summarizes Hall results obtained for several As doped HgCdTe(x=0.3) alloy layers. The results indicate that the carrier concentrations of this set of samples are in the range of $3x10^{17}$-$1.3x10^{15}/cm^3$. The sample MCT115C (using CdTeSe (111) substrate) was annealed under mercury ambient and remained p-type with a carrier concentration of $5.3x10^{15}/cm^3$ at 77K. Hence we believe that the desired electrical properties can be achieved for both p-on-n and n-on-p device structure applications.

We have also measured the minority carrier lifetime of these p-type HgCdTe alloy layers by the photoconductive decay technique at SBRC. The excitation source was step-modulated 632.8 nm HeNe laser. The lifetime measurements were made as function of temperature between 80K and 300K. Tables 9 and 10 list the carrier lifetime of the sample MCT115C and MCT120A in the temperature range of 297-86K. The data show that the carrier lifetime of these samples is about 4 μs at about 90K. The carrier concentration and alloy composition were also measured on these samples in order to properly compare the results with previous measurements on LPE-grown material. The composition and carrier concentration are x=0.32 and $n=5x10^{15}/cm^3$ for MCT115C and x=0.35 and $n=1x10^{16}/cm^3$ for MCT120A sample. The lifetime values are equal to or greater than those observed in comparably doped LPE HgCdTe. These results demonstrated that high quality extrinsically p-type doped material can be grown by MBE.

2.5.6 Indium Doping

We have carried out several sets of experiments on the growth of In-doped n-type HgCdTe(x=0.2) alloy layers. We

TABLE 8. Hall Data of Several As-Doped $Hg_{0.7}Cd_{0.3}Te$ Alloys.

8923-09-09

SAMPLE	Hg ANNEALING	CARRIER CONCENTRATION (/c3)		MOBILITY cm2/V·sec	
		300K	77K	300K	77K
MCT115C	BEFORE	$4.9X10^{16}$	$1.4X10^{16}$	29	38
	AFTER	$5.6X10^{16}$	$5.3X10^{15}$	29	214
MCT120A	BEFORE	$2.9X10^{17}$	$1.7X10^{17}$	40	42
	AFTER	$3X10^{17}$	$2.1X10^{17}$	24	44
MCT123A	BEFORE	$-8.1X10^{15}$	$1.3X10^{15}$	$-2.1X10^{3}$	100
MCT124A	BEFORE	$-9.5X10^{15}$	$5.2X10^{15}$	$-2.5X10^{3}$	77
MCT126A	BEFORE	$-8.7X10^{15}$	$1.5X10^{16}$	$-2.3X10^{3}$	60
MCT128A	BEFORE	$-6.0X10^{15}$	$2.8X10^{16}$	$-1.7X10^{3}$	167

8923-09-06

TABLE 9. PC Lifetime Data for the Sample MCT-115C.

DATA	TEMP. (°K)	PC LIFE (nS)
1	87	3750
2	90	3990
3	100	3400
4	110	3160
5	120	3130
6	130	2970
7	140	2810
8	150	2810
9	160	2620
10	170	2730
11	180	2580
12	190	2420
13	200	2460
14	210	2220
15	220	2010
16	230	2030
17	240	1950
18	250	2030
19	260	2230
20	270	2230
21	280	2420
22	290	2420
23	297	2500

8923-09-08

TABLE 10. PC Lifetime Data for the Sample MCT-120A.

DATA	TEMP. (°K)	PC LIFE (nS)
1	86	4230
2	90	4375
3	100	4260
4	110	3870
5	120	3560
6	130	3590
7	140	3320
8	150	2930
9	160	2340
10	170	1840
11	180	1440
12	190	1090
13	200	976
14	210	1130
15	220	1170
16	230	1370
17	240	1560
18	250	1170
19	260	1020
20	270	1130
21	280	893
22	290	742
23	297	664

believe the results indicate that n-type alloy layers are easier to form than p-type layer because of the efficient incorporation of indium in the mercury (or cadmium) sublattice because of the availability of mercury (or cadmium) vacancies in the materials.

A series of In doped n-type HgCdTe alloy layers were grown with the indium source temperature ranging from 640 to 670°C. Infrared transmission measurements indicated that the compositions of these samples are about x=0.18. Hall data indicated that carrier concentrations of this series of samples are in the range of $1x10^{18}$ to $5x^{17}/cm^3$ with Hall mobilities ranging from 1.5 to $2.4x10^4$ $cm^2/V\cdot s$ at 77K. PC-decay lifetime measurements indicated that these samples have lifetimes <50 ns. This is consistent with the low x value (<0.2) and high doping concentrations in these samples.

Another series of indium doped n-type HgCdTe alloy layers was grown with the indium source temperature ranging from 620 to 640°C. Energy dispersive x-ray analysis indicated that the compositions of these samples were approximately x=0.2. Hall measurements show that the carrier concentrations are in the range of 3.9 to $2.1x10^{17}/cm^3$ with Hall mobilities ranging from 8.3 to $7.4x10^3$ $cm^2/V\cdot s$ at 77K. The data also showed that the carrier concentration of the undoped sample was about $6x10^{15}/cm^3$ at 77K.

Subsequently, a series of indium-doped n-type HgCdTe alloy layers was grown with the indium source temperature ranging from 550 to 580°C. Hall data indicated that carrier concentrations of this series of samples were in the range of 9 to $1x10^{16}/cm^3$ with Hall mobilities about $8x10^3$ $cm^3/V\cdot s$ at 77K. Photoconductive decay measurements indicated that the lifetime of the sample MCT-198D(x=.23, $n=5x10^{16}/cm^3$) is about 650 ns at 77K, which is again equal to or greater than values observed on comparably doped LPE samples. The three series of experimental results are summarized in Table 11 for comparisons. The results suggest that indium source temperature needs to be further decreased and

TABLE 11. Hall Data of In Doped HgCdTe Alloy Layers.

SERIES	CARRIER CONCENTRATION (/cm3) 77 °K	MOBILITY (cm2/V·sec) 77 °K	In Doping Temperature
1	$1x10^{18}$-$5x10^{17}$	1.5-2.4x10^4	640-670
2	$2.1x10^{18}$-$3.9x10^{17}$	7.4-8.3x10^3	600-640
3	$1x10^{16}$-$9x10^{16}$	8x10^3	550-580

the background doping must be minimized for advanced detector applications.

One of the reasons we have difficulty in reducing the indium concentration in our layers is that the system has acquired a certain background level because of indium accumulated in the system from our indium temperature monitoring and the extended use of indium during our series of experiments. This aspect of the problem is being corrected.

SIMS was used to determine the indium concentration in the HgCdTe alloy layers in order to estimate the doping efficiency. For example, Figure 15 shows the SIMS profiles of indium, tellurium, and mercury from the sample MCT-164. The data indicated that: (1) the indium concentration is $2x10^{17}/cm^3$ with uniform distribution in the layer, (2) the indium signal from the substrate is at least three orders of magnitude less than that from the epilayer, (3) the interface between the indium-doped HgCdTe and the undoped substrate is quite abrupt and, (4) the doping efficiency is estimated to be close to 100% according to SIMS and Hall data, which is higher than that reported previously.[11,12]

2.6 DOUBLE LAYER HETEROJUNCTION

A series of simple diode arrays was fabricated and probe tested at 80K. These experiments were designed to

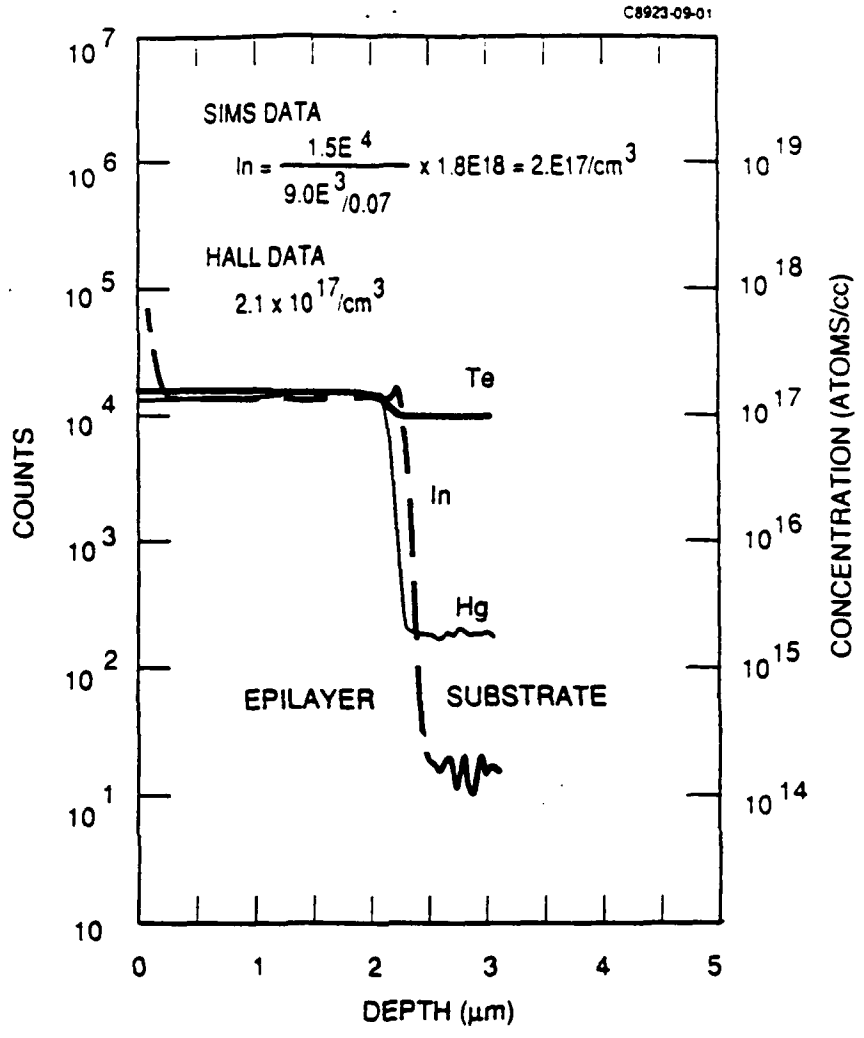

FIGURE 15. SIMS profiles of indium, tellurium, and mercury from the sample MCT-164.

(1) demonstrate double layer heterojunction devices using MBE HgCdTe, (2) verify the incorporation and activation of the impurity dopants in the material, and (3) identify material and growth problems that are affecting the performance of infrared photodiodes. All device fabrication activity in this program was concentrated on the p-on-n DLHJ diode structure. Two approaches are used to form a double layer heterojunction. First is an in-situ approach in which we use MBE technology to grow both the wide band gap (x=0.3) p-type cap layer and the narrow band gap (x=0.2) n-type base layer. Second is a hybrid approach in which we use MBE technology to grow a cap layer on top of an LPE grown base layer. The second approach is especially attractive because it enables us to use the low doped ($<1x10^{15}/cm^3$) LPE layer for the base until we correct our indium memory problem discussed in the previous section.

Several double layer heterojunction structures were grown with a 5 μm n-type base layer and a 1.5 μm p-type cap layer by MBE technology. The cap layers are doped with arsenic and the base layers are either undoped or indium doped. The first iteration of diode (8 mil by 9 mil) fabrication and testing were completed. No rectification was observed from these diodes. The poor device performance was attributed to several factors: (1) difficulties encountered in removing the CdTe passivation from the p-on-n structures (2) the low x value (0.18 rather than 0.22) in the base layer which caused excessive tuning currents, and (3) higher base layer doping concentration than desired for LWIR devices ($>1x10^{15}/cm^3$).

To separate the material factors limiting device performance, MBE As-doped cap layers were grown on LPE indium-doped LWIR base layers. The LPE base layers were known to produce high performance devices. These intermediate experiments were designed to verify the characteristics of the As-doped layers. This iteration of diode fabrication was carried out without CdTe passivation on the double layer

heterostructure. These diodes are expected to have cutoff wavelengths of 9.5 μm at 80K. The probe test results are shown in Figure 16.

Figure 16 shows the i-v characteristics of several diodes from a double layer heterojunction sample (MCT-197E). The layer structure consists of a 2 μm MBE grown As-doped HgCdTe (x=0.3) on a 6 μm LPE grown indium-doped HgCdTe (x=0.22) layer. Rectification was observed, and i-v curves for these devices show excellent reverse breakdown voltages and high short-circuit current. The kink in the i-v curves in forward bias is attributed to a non-ohmic contact on the p-type MBE HgCdTe. These results established the validity of the As-doped p-type MBE materials.

To understand the junction characteristics and doping profile, SIMS analysis was performed on this sample. Figure 17 shows the indium, arsenic, mercury, cadmium and tellurium profiles from this hybrid double layer structure. The data show that the MBE-grown cap layer has As doping concentration at $5x10^{16}/cm^3$ and the LPE-grown base layer has indium doping concentration at $1x10^{15}/cm^3$. It is interesting to note that the arsenic concentration is about two orders of magnitude higher on the surface compared with that in the layer, and the indium concentration is about one order magnitude higher at the interface of MBE/LPE layers compared with the concentration in the base layer. We believe that the higher magnitude is a result of the enhancement of secondary ion yield which is caused by the presence of surface and interface oxides. This data also suggest that the oxides on the LPE-grown HgCdTe need to be completely removed for optimal performance from this device.

The SIMS profile shows that the indium concentration is about $2x10^{15}/cm^3$ in the cap layer, which is higher than that of indium-doped LPE grown base layer by a factor of 4. This is not surprising because of the large number of indium chips used in our temperature calibration resulting in the memory effect in

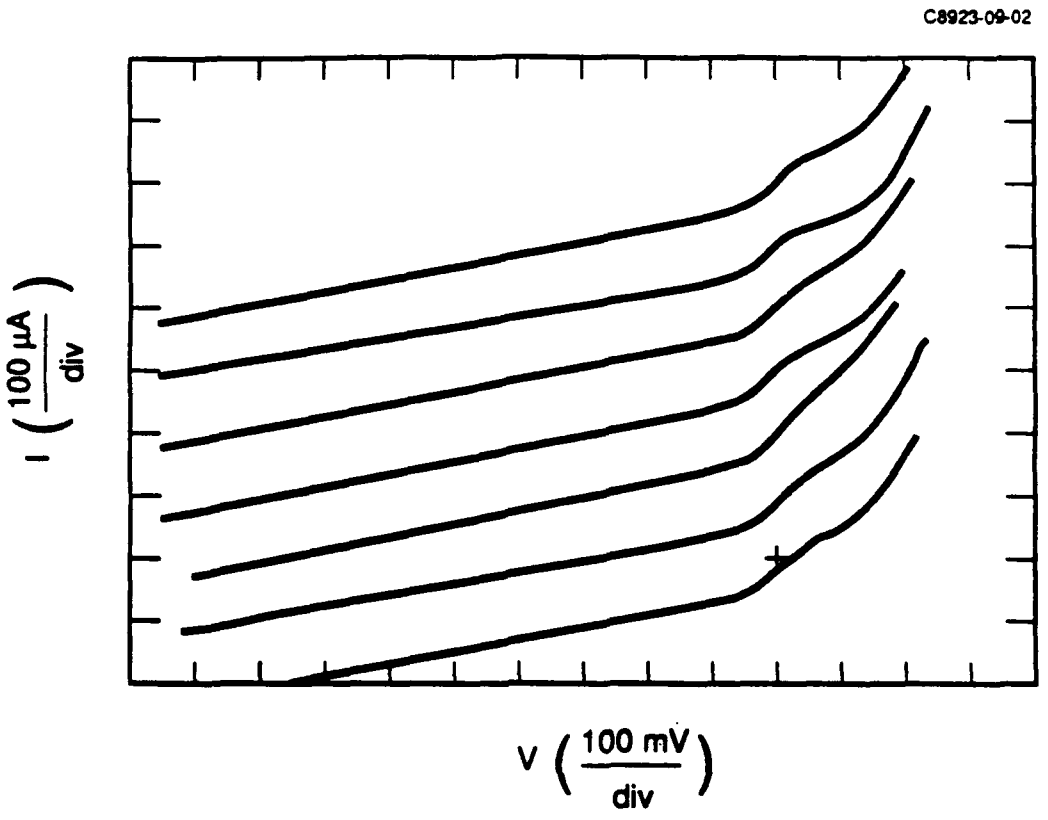

FIGURE 16. 80K probe data for LWIR p-on-n diodes with MBE cap layer on LPE base layer (MCT 197E).

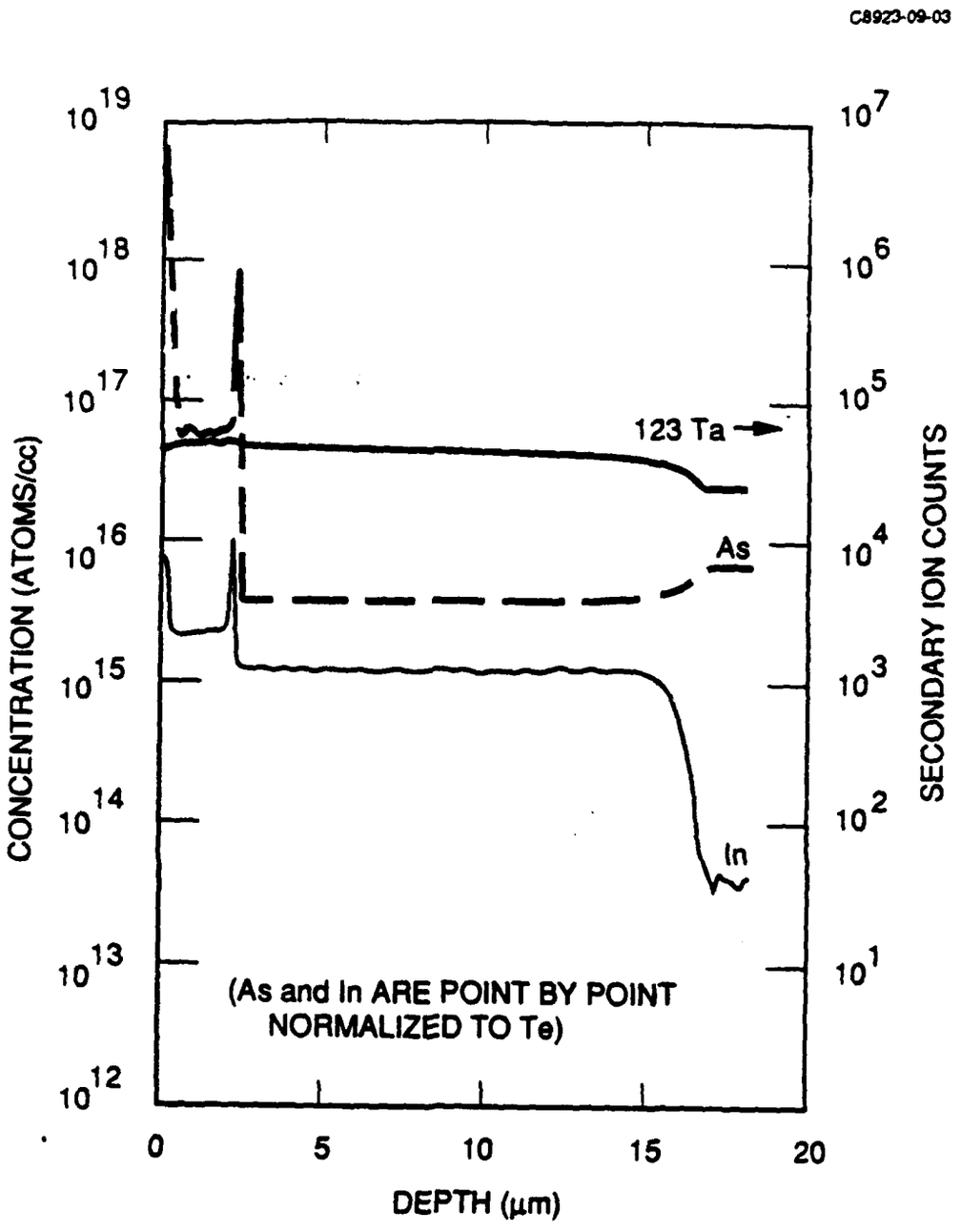

FIGURE 17. SIMS profile of the sample MCT 197E indicating (a) the MBE grown cap layer has As doping concentration at $5x10^{16}/cm^3$ and (2) the LPE grown base layer has In doping concentration at $1x10^{15}/cm^3$.

our chamber. We are currently developing alternative techniques to monitor the surface temperature during the growth run. The SIMS results also show excellent detection sensitivities for arsenic and indium with an oxygen primary beam; they are about $5x10^{15}/cm^3$ and $4x10^{13}/cm^3$ for arsenic and indium, respectively.

Following the successful results using the LPE base material, we again attempted to fabricate devices using a complete MBE structure. The device fabrication for these diodes was performed as a part of SBRC's N339 IR&D project. This double layer structure (MCT-202A) consists of a 1.5 μm MBE grown arsenic p-type layer (x=0.3) on a 4 μm MBE-grown indium n-type layer (x=0.2). The probe test results are shown in Figure 18. These diodes exhibited rectification indicating the presence of a junction. However the devices did not exhibit measurable photocurrent and also showed relatively low breakdown voltages. These effects may be the result of the base doping concentration being higher than desired ($>1x10^{16}/cm^3$). The high doping concentration will lead to excessive tunneling currents that will cause the poor breakdown characteristics. The high doping concentration will also cause heterojunction barriers to form that can limit the optical response of the diodes.

Secondary ion mass spectroscopy (SIMS) profiles were obtained on the MCT-202A sample. The data shown in Figure 19 indicates that the arsenic and indium doping concentrations are about $3x10^{16}/cm^3$ and $2x10^{16}/cm^3$ respectively. The indium unintentional doping in the cap layer and the intentional doping in the base layer are apparently too high for optimal device operation (as discussed above). Procedures are being instituted to correct this problem.

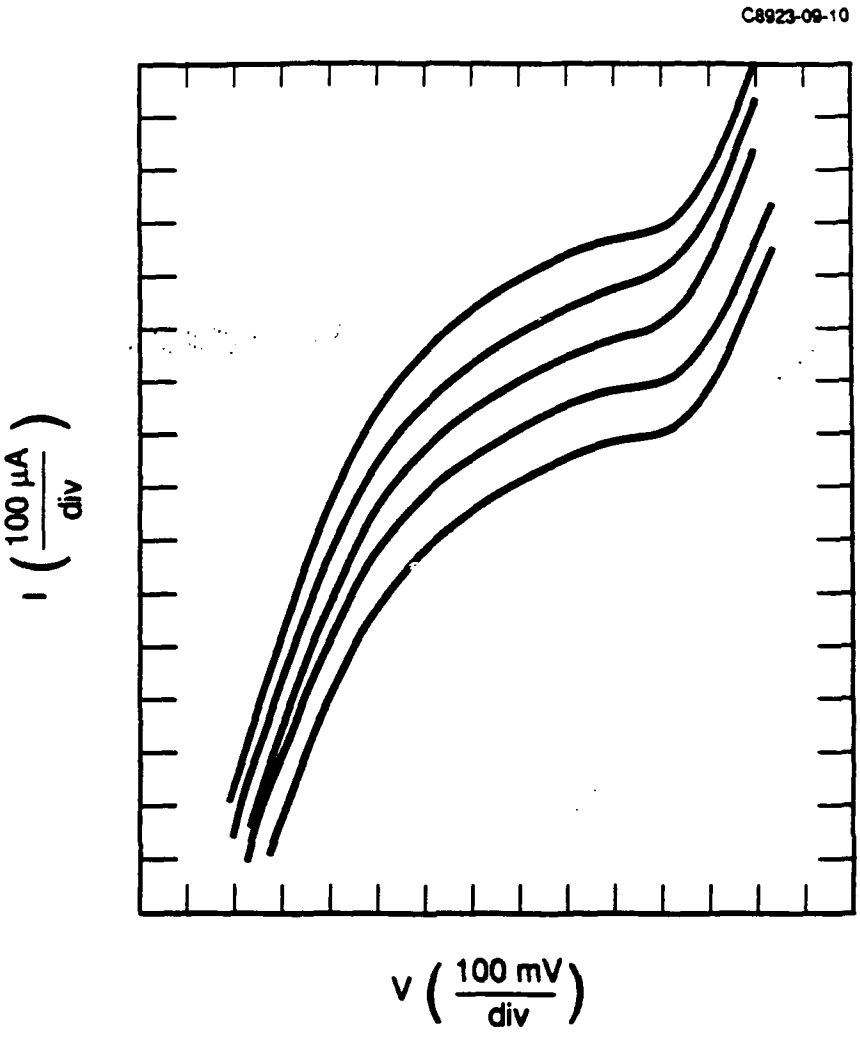

FIGURE 18. 80K probe data for MBE grown p-on-n diodes (MCT-202A).

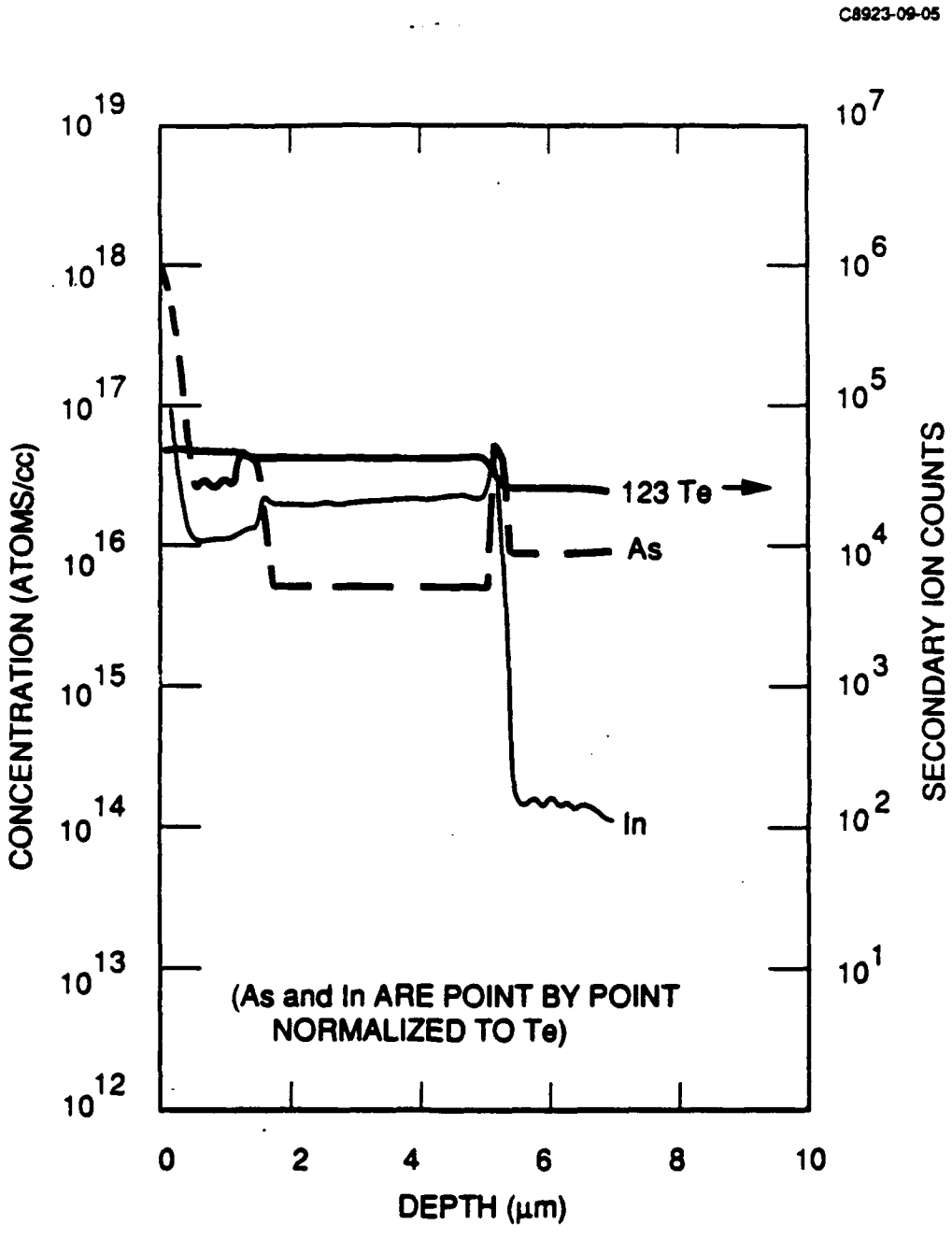

FIGURE 19. SIMS profile of the sample 202A indicating that the As and In doping concentration are about $3x10^{16}$ and $2x10^{16}/cm^3$ respectively.

SECTION 3

CONCLUSIONS AND RECOMMENDATIONS

3.1 CONCLUSIONS

We have established a strong HgCdTe MBE capability at HRL and have demonstrated the growth of CdTe, HgTe, and HgCdTe alloy layers with indium for n-type, and arsenic for p-type. Several initial double layer heterojunction structures have been grown by two approaches, including the in-situ MBE and the MBE-LPE hybrid approach. The p-n junction was demonstrated. Several 8 mil by 9 mil diodes were fabricated, and their junction characteristics were evaluated.

The problem of reproducibility and control are especially difficult in the narrow band gap ternary because it requires the base layer doping to be in the $10^{14}/cm^3$ range for optimum device performance, especially in the long wavelength detector required (10 μm) for programs such as ALICAT. The initial results in our program, however, are extremely encouraging, and we feel that a heterojunction detector with reproducible control can be fabricated by growing the structure below 200°C minimizing many of the problems which have severely limited HgCdTe performance.

3.2 RECOMMENDATIONS FOR FUTURE WORK

Substrate temperature is one of the most critical process parameters in the HgCdTe MBE growth because it controls both the stoichiometry and electrical properties. A better substrate mounting device and temperature monitoring system should be developed for a reproducible growth process.

Control of residual impurities is another important issue for the MBE growth of double layer heterojunction structures. A better vacuum environment with capability of achieving an unintentional doping level at $10^{14}/cm^3$ is necessary for controlled chemical doping of HgCdTe at low levels. More frequent bakeout of the system and purification by outgassing of the source materials in a separate chamber will improve the conditions for a more reproducible process.

REFERENCES

1. E.R. Gertner, Mater. Res. Soc. Symp. Proc. **90**, 357 (1988).

2. H.R. Vydyanath, J.A. Ellsworth, and C.M. Devaney, J. Electron. Mater. **16**, 13 (1987).

3. B.A. Joyce, H. Phys. Chem. Solids **49**, 237 (1988).

4. DARPA II-VI Materials and Processing Conf. Proc., April 7-9 1987.

5. S. Sivananthan, X. Chu, and J.P. Faurie, J. Vac. Sci. Technol. **B5**, 694 (1987).

6. T. Tung, J. Cryst. Growth **86**, 161 (1988).

7. R.N. Bicknell, N.C. Giles, and J.F. Schetzina, Appl. Phys. Lett. **49**, 1096 (1986).

8. R.N. Bicknell, N.C. Giles, J.F. Schetzina, and C. Hitzman, J. Vac. Sci. Technol. **A5**, 3059 (1987).

9. J.D. Benson and C.J. Summers, to be published in J. Cryst. Growth.

10. DARPA II-VI Materials and Processing Conf., April 1988.

11. M. Boukerche, P.S. Wijewrnasuriya, S. Sivananthan, I.K. Sou, Y.J. Kim, K.K. Mahavadi, and J.P. Faurie, J. Vac. Sci. Technol. **A6**, 2830 (1988).

12. M. Boukerche, J. Reno, I.K. Sou, C. Hsu, and J.P. Faurie, Appl. Phys. Lett. **48**, 1733 (1986).

13. M.L. Wroge, D.J. Peterson, B.J. Morris, D.J. Leopold and J.G. Broerman, J. Vac. Sci. Technol. **A6**, 2826 (1988).

14. E.S. Johnson and J.L. Schmit, J. Elect. Mater. **6**, 25 (1977).

15. J.W. Han, S. Hwang, Y Lansari, R.L. Harper, Z. Yang, N.C. Giles, J.W. Cook, Jr., J.F. Schetzina, and S. Sen Appl. Phys. Lett. **54** (1) 1989 p. 63.

TABLE 8. Hall Data of Several As-Doped $Hg_{0.7}Cd_{0.3}Te$ Alloys.

8923-09-09

SAMPLE	Hg ANNEALING	CARRIER CONCENTRATION (/c3)		MOBILITY cm2/V·sec	
		300K	77K	300K	77K
MCT115C	BEFORE	$4.9X10^{16}$	$1.4X10^{16}$	29	38
	AFTER	$5.6X10^{16}$	$5.3X10^{15}$	29	214
MCT120A	BEFORE	$2.9X10^{17}$	$1.7X10^{17}$	40	42
	AFTER	$3X10^{17}$	$2.1X10^{17}$	24	44
MCT123A	BEFORE	$-8.1X10^{15}$	$1.3X10^{15}$	$-2.1X10^{3}$	100
MCT124A	BEFORE	$-9.5X10^{15}$	$5.2X10^{15}$	$-2.5X10^{3}$	77
MCT126A	BEFORE	$-8.7X10^{15}$	$1.5X10^{16}$	$-2.3X10^{3}$	60
MCT128A	BEFORE	$-6.0X10^{15}$	$2.8X10^{16}$	$-1.7X10^{3}$	167

8923-09-06

TABLE 9. PC Lifetime Data for the Sample MCT-115C.

DATA	TEMP. (°K)	PC LIFE (nS)
1	87	3750
2	90	3990
3	100	3400
4	110	3160
5	120	3130
6	130	2970
7	140	2810
8	150	2810
9	160	2620
10	170	2730
11	180	2580
12	190	2420
13	200	2460
14	210	2220
15	220	2010
16	230	2030
17	240	1950
18	250	2030
19	260	2230
20	270	2230
21	280	2420
22	290	2420
23	297	2500

8923-09-08

TABLE 10. PC Lifetime Data for the Sample MCT-120A.

DATA	TEMP. (°K)	PC LIFE (nS)
1	86	4230
2	90	4375
3	100	4260
4	110	3870
5	120	3560
6	130	3590
7	140	3320
8	150	2930
9	160	2340
10	170	1840
11	180	1440
12	190	1090
13	200	976
14	210	1130
15	220	1170
16	230	1370
17	240	1560
18	250	1170
19	260	1020
20	270	1130
21	280	893
22	290	742
23	297	664

believe the results indicate that n-type alloy layers are easier to form than p-type layer because of the efficient incorporation of indium in the mercury (or cadmium) sublattice because of the availability of mercury (or cadmium) vacancies in the materials.

A series of In doped n-type HgCdTe alloy layers were grown with the indium source temperature ranging from 640 to 670°C. Infrared transmission measurements indicated that the compositions of these samples are about x=0.18. Hall data indicated that carrier concentrations of this series of samples are in the range of $1x10^{18}$ to $5x^{17}/cm^3$ with Hall mobilities ranging from 1.5 to $2.4x10^4$ $cm^2/V\cdot s$ at 77K. PC-decay lifetime measurements indicated that these samples have lifetimes <50 ns. This is consistent with the low x value (<0.2) and high doping concentrations in these samples.

Another series of indium doped n-type HgCdTe alloy layers was grown with the indium source temperature ranging from 620 to 640°C. Energy dispersive x-ray analysis indicated that the compositions of these samples were approximately x=0.2. Hall measurements show that the carrier concentrations are in the range of 3.9 to $2.1x10^{17}/cm^3$ with Hall mobilities ranging from 8.3 to $7.4x10^3$ $cm^2/V\cdot s$ at 77K. The data also showed that the carrier concentration of the undoped sample was about $6x10^{15}/cm^3$ at 77K.

Subsequently, a series of indium-doped n-type HgCdTe alloy layers was grown with the indium source temperature ranging from 550 to 580°C. Hall data indicated that carrier concentrations of this series of samples were in the range of 9 to $1x10^{16}/cm^3$ with Hall mobilities about $8x10^3$ $cm^3/V\cdot s$ at 77K. Photoconductive decay measurements indicated that the lifetime of the sample MCT-198D(x=.23, $n=5x10^{16}/cm^3$) is about 650 ns at 77K, which is again equal to or greater than values observed on comparably doped LPE samples. The three series of experimental results are summarized in Table 11 for comparisons. The results suggest that indium source temperature needs to be further decreased and

TABLE 11. Hall Data of In Doped HgCdTe Alloy Layers.

SERIES	CARRIER CONCENTRATION (/cm3) 77 °K	MOBILITY (cm^2/V sec) 77 °K	In Doping Temperature
1	$1x10^{18}$-$5x10^{17}$	1.5-2.4x10^4	640-670
2	2.1x10^{18}-3.9x10^{17}	7.4-8.3x10^3	600-640
3	1x10^{16}-9x10^{16}	8x10^3	550-580

the background doping must be minimized for advanced detector applications.

One of the reasons we have difficulty in reducing the indium concentration in our layers is that the system has acquired a certain background level because of indium accumulated in the system from our indium temperature monitoring and the extended use of indium during our series of experiments. This aspect of the problem is being corrected.

SIMS was used to determine the indium concentration in the HgCdTe alloy layers in order to estimate the doping efficiency. For example, Figure 15 shows the SIMS profiles of indium, tellurium, and mercury from the sample MCT-164. The data indicated that: (1) the indium concentration is $2x10^{17}/cm^3$ with uniform distribution in the layer, (2) the indium signal from the substrate is at least three orders of magnitude less than that from the epilayer, (3) the interface between the indium-doped HgCdTe and the undoped substrate is quite abrupt and, (4) the doping efficiency is estimated to be close to 100% according to SIMS and Hall data, which is higher than that reported previously.[11,12]

2.6 DOUBLE LAYER HETEROJUNCTION

A series of simple diode arrays was fabricated and probe tested at 80K. These experiments were designed to

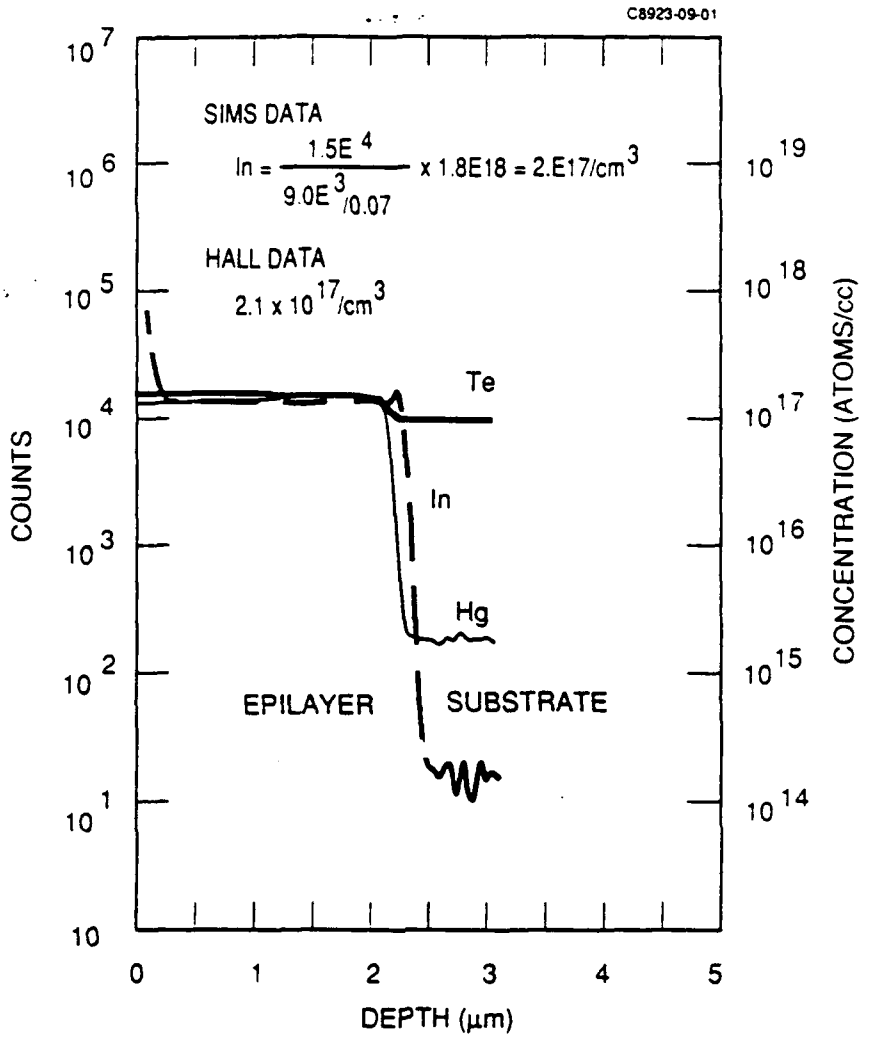

FIGURE 15. SIMS profiles of indium, tellurium, and mercury from the sample MCT-164.

(1) demonstrate double layer heterojunction devices using MBE HgCdTe, (2) verify the incorporation and activation of the impurity dopants in the material, and (3) identify material and growth problems that are affecting the performance of infrared photodiodes. All device fabrication activity in this program was concentrated on the p-on-n DLHJ diode structure. Two approaches are used to form a double layer heterojunction. First is an in-situ approach in which we use MBE technology to grow both the wide band gap (x=0.3) p-type cap layer and the narrow band gap (x=0.2) n-type base layer. Second is a hybrid approach in which we use MBE technology to grow a cap layer on top of an LPE grown base layer. The second approach is especially attractive because it enables us to use the low doped ($<1x10^{15}/cm^3$) LPE layer for the base until we correct our indium memory problem discussed in the previous section.

Several double layer heterojunction structures were grown with a 5 μm n-type base layer and a 1.5 μm p-type cap layer by MBE technology. The cap layers are doped with arsenic and the base layers are either undoped or indium doped. The first iteration of diode (8 mil by 9 mil) fabrication and testing were completed. No rectification was observed from these diodes. The poor device performance was attributed to several factors: (1) difficulties encountered in removing the CdTe passivation from the p-on-n structures (2) the low x value (0.18 rather than 0.22) in the base layer which caused excessive tuning currents, and (3) higher base layer doping concentration than desired for LWIR devices ($>1x10^{15}/cm^3$).

To separate the material factors limiting device performance, MBE As-doped cap layers were grown on LPE indium-doped LWIR base layers. The LPE base layers were known to produce high performance devices. These intermediate experiments were designed to verify the characteristics of the As-doped layers. This iteration of diode fabrication was carried out without CdTe passivation on the double layer

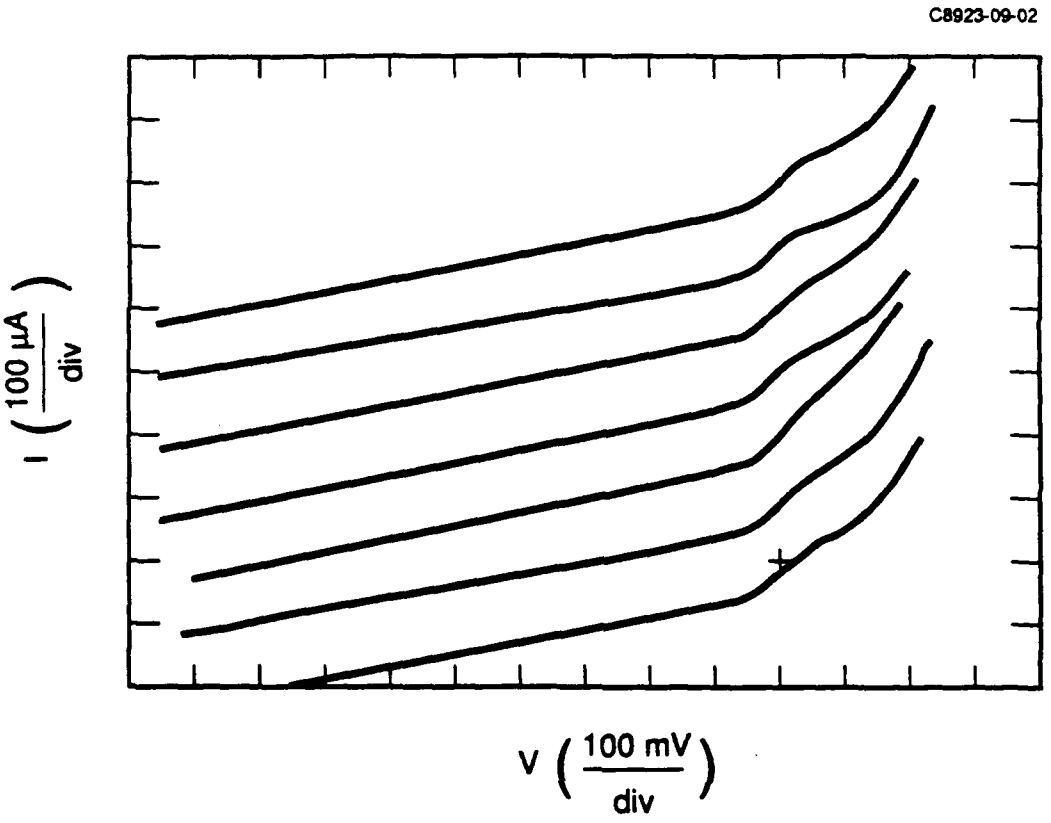

FIGURE 16. 80K probe data for LWIR p-on-n diodes with MBE cap layer on LPE base layer (MCT 197E).

REFERENCES

1. E.R. Gertner, Mater. Res. Soc. Symp. Proc. **90**, 357 (1988).

2. H.R. Vydyanath, J.A. Ellsworth, and C.M. Devaney, J. Electron. Mater. **16**, 13 (1987).

3. B.A. Joyce, H. Phys. Chem. Solids **49**, 237 (1988).

4. DARPA II-VI Materials and Processing Conf. Proc., April 7-9 1987.

5. S. Sivananthan, X. Chu, and J.P. Faurie, J. Vac. Sci. Technol. **B5**, 694 (1987).

6. T. Tung, J. Cryst. Growth **86**, 161 (1988).

7. R.N. Bicknell, N.C. Giles, and J.F. Schetzina, Appl. Phys. Lett. **49**, 1096 (1986).

8. R.N. Bicknell, N.C. Giles, J.F. Schetzina, and C. Hitzman, J. Vac. Sci. Technol. **A5**, 3059 (1987).

9. J.D. Benson and C.J. Summers, to be published in J. Cryst. Growth.

10. DARPA II-VI Materials and Processing Conf., April 1988.

11. M. Boukerche, P.S. Wijewrnasuriya, S. Sivananthan, I.K. Sou, Y.J. Kim, K.K. Mahavadi, and J.P. Faurie, J. Vac. Sci. Technol. **A6**, 2830 (1988).

12. M. Boukerche, J. Reno, I.K. Sou, C. Hsu, and J.P. Faurie, Appl. Phys. Lett. **48**, 1733 (1986).

13. M.L. Wroge, D.J. Peterson, B.J. Morris, D.J. Leopold and J.G. Broerman, J. Vac. Sci. Technol. **A6**, 2826 (1988).

14. E.S. Johnson and J.L. Schmit, J. Elect. Mater. **6**, 25 (1977).

15. J.W. Han, S. Hwang, Y Lansari, R.L. Harper, Z. Yang, N.C. Giles, J.W. Cook, Jr., J.F. Schetzina, and S. Sen Appl. Phys. Lett. **54** (1) 1989 p. 63.